A general description of a gravity current front propagating in a two-layer stratified fluid

Brian L. White[1]† and Karl R. Helfrich[2]

[1] Marine Sciences Department, UNC–Chapel Hill, NC 27599, USA

[2] Department of Physical Oceanography, Woods Hole Oceanographic Institution, Woods Hole, MA 02543, USA

The behaviour of a gravity current propagating into a two-layer stratified ambient fluid is described in detail. A comprehensive description is given of the different flow regimes, with particular emphasis on the front condition linking the thickness of the gravity current to its speed of propagation and the transfer of energy to upstream disturbances in the form of internal bores and nonlinear solitary waves. Hydraulic theory analogous to that of two-layer flow over topography (Baines, *J. Fluid Mech.*, vol. 146, 1984, pp. 127–167) is extended to the gravity current problem to classify frontal behaviour into the following regimes: Type I, subcritical currents; Type II, currents that generate upstream undular bores; Type III, currents that generate an upstream monotonic bore connected by a rarefaction; Type IV, supercritical fronts with a large-amplitude trapped solitary-wave-like disturbance; and Type V, supercritical gravity currents. Over 200 two-dimensional Boussinesq–Euler simulations spanning a range of gravity current properties demonstrate good agreement, for both the behavioural regime and the front condition $U_o(h)$, with hydraulic theory that extends original work by Rottman & Simpson (*Q. J. R. Meteorol. Soc.*, vol. 115, 1989, pp. 941–963) to arbitrary ambient layer thickness, and uses an improved closure for the upstream bore that correctly predicts the behaviour in the limit of large bore amplitude. In addition, the energy balance is analysed, and it is shown that the energy transfer from the gravity current to upstream disturbances is significant, and consistent with the hydraulic theory. The results demonstrate a clear connection to the problem of upstream resonance in two-layer flow over topography, and have significant implications for interpreting field observations of nonlinear internal waves generated by atmospheric density currents and coastal river plumes.

Key words: gravity currents, hydraulic control, internal waves

---

1. Introduction

The propagation of a gravity current into a stably stratified ambient is a common process in the atmosphere and ocean, with implications for mixing and energy transfer. Ambient stratification may act as a waveguide, supporting the generation and propagation of internal waves near the gravity current front. Two examples are the well-known Morning Glory in Australia, an atmospheric undular bore (Rottman & Simpson 1989), and the Columbia River plume, where observations have shown

† Email address for correspondence: bwhite@unc.edu

regular generation of large-amplitude waves ahead of the front (Nash & Moum 2005; Kilcher & Nash 2010). Nash & Moum explained these observations by drawing an analogy to hydraulic resonance in stratified flow over topography (Grimshaw & Smyth 1986; Melville & Helfrich 1987; Lamb 1994; Farmer & Armi 1999). In support of that hypothesis, White & Helfrich (2008) demonstrated that a gravity current of thickness h propagating into ambient stratification can produce upstream-propagating disturbances in parameter regimes matching hydraulic resonance by topography of an equivalent height. However, the gravity current problem is even more complex than topography, because the front is a free boundary which is deformed by the internal wave motion.

At the Columbia plume front, where the freshwater source flows into stratified shelf waters with a very thin upper layer, a rich set of dynamics has been observed, including upstream radiation of nonlinear internal waves or a single large-amplitude head wave trapped at the front. In each case, the amplitudes of these frontal disturbances are as large as tens of metres, where the average upper-layer thickness is only of the order of 5 m and very high rates of turbulent kinetic energy dissipation have been observed (Moum, Nash & Klymak 2008; Nash, Kilcher & Moum 2009; Kilcher & Nash 2010). Recent work has addressed the influence of waves on the front evolution, and wave generation (Kilcher & Nash 2010; Stashchuk & Vlasenko 2009). Pan & Jay (2009) suggested that the nonlinear internal waves may contain as much as 70 % of the energy in the Columbia near-front region.

Nash & Moum (2005) hypothesized that internal waves were generated from the Columbia plume when the front speed, U_o, which slows on the shelf due to a combination of rotational, tidal, and spreading effects, becomes subcritical to the linear long wave speed in the ambient stratification, c_o, i.e. the Froude number is less than one, $Fr = U_o/c_o < 1$. This approach described their observations fairly well. Supporting this interpretation is experimental work by Maxworthy *et al.* (2002), who studied dense gravity currents generated by lock release in a uniformly stratified ambient (constant Brunt–Väisälä frequency, N). They found that a critical Froude number based on the gravity current speed, U_o, of $Fr = U_o/(NH/\pi) = 1$ described a transition from a supercritical current with constant front speed to a subcritical regime in which internal waves were generated at the front and carried dense fluid ahead of the current.

However, a wide body of work on hydraulic control and resonance in stratified flow over topography (see Baines 1995) has shown that in general there is a range of $Fr = U_o/c_o \approx 1$ for which upstream disturbances may be generated. Within this transcritical band, there can be a resonant transfer of energy from the barotropic flow over the topography into the ambient waveguide, producing nonlinear internal waves and upstream bores (Grimshaw & Smyth 1986; Melville & Helfrich 1987). One approach to the transcritical resonance problem uses weakly nonlinear theory, either the forced KdV or extended KdV equation to predict the transcritical Fr range in which upstream resonance is expected (Grimshaw & Smyth 1986; Melville & Helfrich 1987; Grimshaw, Chan & Chow 2002). These approaches include dispersion, but not the full nonlinearity. This contrasts, for example, with the approach of Baines (1984), which uses hydraulic theory to connect regions of uniform flow over topography, capturing the full nonlinearity but not dispersion.

Rottman & Simpson (1989) studied gravity currents propagating into two-layer stratification and found that some solutions generated an upstream undular bore, characterized by a wave train near the front, while others were supercritical. They interpreted their results in terms of hydraulic resonance by topography, in the same manner as Baines (1984). This allowed a prediction of the transition between

gravity currents that were subcritical, supercritical, or generated undular bores. They also used a theory first proposed by Crook (1983), to connect the speed of the upstream propagating bore with that of the gravity current front in a two-layer fluid with infinitely thick upper layer. However, the limited data did not allow a full exploration of the transitions between gravity current regimes that were either subcritical, supercritical, or generated undular bores.

In this paper, we take a similar approach to Baines (1984) and Rottman & Simpson (1989) to describe gravity currents in two-layer stratification using fully nonlinear hydraulic theory. We present a new theory for the gravity current front speed in sub-, super-, and transcritical resonant regimes by developing an improved jump condition linking the gravity current front to an upstream undular bore, and we generalize the results to arbitrary ambient layer thicknesses. A substantial set of two-dimensional Boussinesq–Euler simulations demonstrates the validity of the approach and its ability to delineate between frontal regimes. Finally, we explore the energy exchange between the gravity current front and the upstream waves. Ungarish & Huppert (2006), in an analysis for uniform stratification, suggested that the exchange between a gravity current and upstream waves should be small, but the energy flux estimates for the Columbia plume (Pan & Jay 2009) contradict this hypothesis. We show that there is in fact an appreciable energy exchange between the front and the waves in the transcritical regime.

We begin in §2 by summarizing the existing theory that links steady hydraulic solutions of gravity currents in stratification to the theory of nonlinear internal waves and resonance by topography. In §3 we develop a new theory that predicts the gravity current front speed in the regime where an upstream bore is generated. In §4 we describe two-dimensional numerical simulations of gravity currents generated by a dam-break, and describe five regimes of frontal behaviour exhibited. In §6 we compare the hydraulic theory with the numerical results and find that the theory predicts both the observed frontal regime and front speed relationship, $U_o(h)$. Finally, in §7 we analyse the energy transfer between the gravity current and the upstream bore, and demonstrate that the hydraulic theory and simulation results agree quite well. The results suggest that the energy transfer to upstream disturbances can require a significant fraction of the total gravity current energy flux.

2. Gravity currents in a stratified ambient: problem description and existing theory

The presence of ambient stratification modifies the classic problem of a gravity current produced by lock-exchange (Benjamin 1968; Simpson 1997), in which a mass of dense (or light) fluid propagates into a lighter (heavier) ambient fluid until arrested by friction or boundaries. Benjamin (1968) found steady solutions to the lock-exchange problem without ambient stratification, including a special energy-conserving solution when the gravity current occupies exactly half the total fluid depth. Stratification produces a richer set of behaviours because long internal waves can propagate in the ambient waveguide ahead of the current and exchange energy with the current.

2.1. *Problem set-up*

A depiction of the problem considered is shown in figure 1. A volume (lock) of fluid with height h_d, length L_d and density ρ_c collapses into a two-layer ambient of uniform depth H and densities $\rho_{1,2}$ in the lower and upper layers, respectively, of
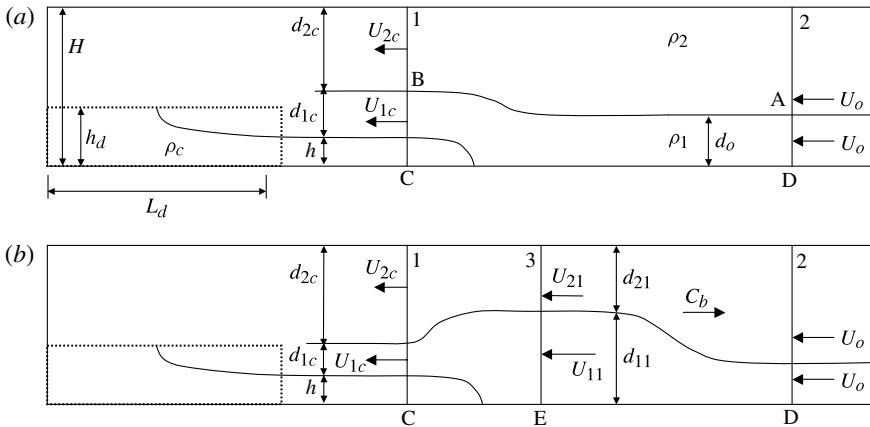
FIGURE 1. Description of gravity current problem. (*a*) Steady gravity current with height h, initial dam height h_d, length L_d, and density ρ_c. The bottom and top layer densities are ρ_1 and ρ_2 in a layer of total depth H and bottom layer thickness d_o. The layer depths over the gravity current are d_{1c} and d_{2c} and the velocities are U_{1c} and U_{2c}. A, B, C and D are points on the control volume used for momentum and energy conservation. (*b*) Gravity current with upstream bore. The bore speed is C_b in a frame moving with the current speed U_o, the bore amplitude is d_{11} and the velocities through the bore are U_{11} and U_{21}.

thickness d_o and $H - d_o$. The release produces a gravity current with thickness h and speed U_o which may also excite waves in the ambient ahead. The strength of the gravity current relative to the ambient stratification is described by the parameter $S \equiv (\rho_1 - \rho_2)/(\rho_c - \rho_2)$. Throughout the paper we apply the Boussinesq approximation, define a reference density $\rho_o \equiv \rho_2$ and define the reduced gravity $g' = g(\rho_1 - \rho_2)/\rho_2$. Note that for a free-slip bottom and in the Boussinesq limit, the dense current is identical to a surface current with an equivalent buoyancy deficit (the river plume case).

2.2. *Gravity currents in a continuously stratified ambient*

Ungarish (2006) developed a theory for the steady front speed of a gravity current propagating in a uniform (constant N) ambient by treating the dense current, with thickness h, as topography of equivalent height. The displacement of the ambient density field was calculated using Long's method (see Baines 1995). White & Helfrich (2008) developed a general theory for steady gravity currents in arbitrary stratification. They used a one-dimensional version of the nonlinear Dubriel–Jacotin–Long (DJL) equation, applied to nonlinear internal waves with trapped cores by Lamb & Wilkie (2004). The solutions, which link the uniform hydrostatic regions above the current and in the undisturbed ambient by a jump condition, can be found only for certain combinations of the current thickness, front speed, and ambient stratification. Given the ambient density profile, there also exists a unique solution in (h, U_o), termed the conjugate state, that is energy-preserving. In general, solutions break down, implying upstream wave generation, when the front speed, U_o, is less than the long wave speed in the stratified ambient above the dividing gravity current streamline, c_l. For non-uniform N, $c_l > c_o$, which means that a critical Froude number for wave generation $U_o/c_l = 1$ is preferable to the often-cited $Fr = U_o/c_o = 1$ condition. In fact, there is

a transcritical resonant band around $Fr = 1$ in which waves are generated, as we will show in this paper for two-layer stratification.

2.3. *Connection between conjugate gravity currents, nonlinear internal waves and internal bores*

Because there is a strong connection between the conjugate state gravity current solutions and nonlinear internal waves, some background on the latter is appropriate. Using DJL theory, Stastna & Lamb (2002) found solutions for mode-one solitary waves in continuous stratification, steady in a frame of reference moving with the wave speed c. Lamb (2002) showed that the wave amplitude increases with c until one of three limiting outcomes is realized (depending on the ambient stratification and background shear). The first is the development of a shear instability as the Richardson number in the wave frame drops below a critical value. A second possibility is a breaking limit, the onset of which occurs when the the local velocity within the wave matches the speed of wave propagation, i.e. $u = 0$ in the wave frame ($u = c$ in the laboratory frame) at $z = 0$ ($z = 1$) for waves of elevation (depression). A necessary condition for this overturning limit is that N be non-zero at the boundary, i.e. $z = 0$ ($z = 1$) for waves of elevation (depression) (Lamb 2002). In the third limit, if $N = 0$ at the boundary, solutions may instead reach a limiting flat-top internal wave, termed the conjugate state by Lamb (2002). This solution is an energy-conserving internal bore that links the upstream and downstream flow. In the two-layer Boussinesq limit, Lamb (2000) showed that the conjugate state speed is $C_{cs} = 0.5 (g'H)^{1/2}$, and the upstream pycnocline depth is found at mid-depth $h_{cs} = H/2$, both independent of the undisturbed layer depth, d_o. This theory is particularly relevant to gravity currents in two-layer ambients because the condition $N = 0$ at the boundaries implies that the conjugate state is the limiting large-amplitude wave, and the overturning limit is not reached.

If $N \neq 0$ near the boundary, internal waves reach the breaking limit, eventually producing a wave with a trapped core of recirculating fluid. Models have been suggested for waves with trapped cores (Derzho & Grimshaw 1997; Brown & Christie 1998; Helfrich & White 2010; King, Carr & Dritschel 2010). Lamb & Wilkie (2004) found conjugate flow solutions for waves with a trapped core of uniform density and arbitrary uniform vorticity, applying the DJL equation outside the core. These solutions, like the conjugate bore, are energy-conserving, and can be viewed as conjugate states with the inclusion of trapped fluid with density equal to the density on the boundary (equivalent to $S = 1$). White & Helfrich (2008) showed that these solutions provide the link to gravity currents in ambient stratification. They extended the theory to arbitrary core density ($S \neq 1$) and showed that the resulting conjugate state solutions described the large-lock-height upper limit for steady gravity currents. In the limit $S \rightarrow 0$, the conjugate state recovers Benjamin's energy-conserving half-depth gravity current solution.

2.4. *Gravity currents in two-layer stratification*

An important result of the theory of White & Helfrich (2008) is that gravity current solutions with arbitrary core density ρ_c exist even for ambient density profiles with $N = 0$ at the boundary. In the limit of two-layer stratification, gravity current solutions exist if the core density is below a critical value, such that $S < S_c$, where the critical value of the stratification parameter, S_c, depends on the lower-layer depth, d_o. For $S > S_c$, however, there are no steady gravity current solutions, and the monotonic conjugate bore corresponding to the two-layer stratification, with speed C_{cs} (Lamb 2002, described in § 2.3), is the fastest wave in the system. As a result, this bore

would be expected to travel faster than and extract energy from a trailing gravity current. For $S < S_c$, steady gravity current solutions exist with propagation speeds faster than the conjugate bore, and no upstream energy flux is possible. On this basis, Stastna & Peltier (2005) argued that C_{cs} is the appropriate upper limit for resonance in two-layer flow over topography, which our results will also confirm for resonance at a gravity current front.

In seminal work, Holyer & Huppert (1980) presented a theory for gravity current propagation speed in a two-layer stratified ambient, which provides a direct link to the generalized conjugate gravity current theory. They found solutions for front speed given the upstream layer depths, and for currents that are either energy-conserving or dissipative. Their energy-conserving solutions correspond to the two-layer conjugate state gravity current solutions. Here their theory is briefly reviewed. First, assume the gravity current is steady in a reference frame moving with speed U_o. Further, assume that the flow is uniform and the pressure hydrostatic in the region behind the gravity current front and in the ambient region upstream (these vertical sections are denoted 1 and 2, respectively, in figure 1). Applying conservation of mass, momentum, and energy yields the gravity current speed, U_o, as a function of h. Here we assume the Boussinesq limit for simplicity, although the more general Holyer & Huppert theory does not have such a restriction.

First, conservation of mass between the upstream and the flow over the current gives

$$U_{1c} = U_o d_o / d_{1c} \tag{2.1}$$

and

$$U_{2c} = U_o (H - d_o) / (H - d_{1c} - h). \tag{2.2}$$

The Bernoulli equation along the interface between the lower and upper ambient layers, respectively, (referring to the points A, B, C and D in figure 1a) gives

$$p_A + \tfrac{1}{2}\rho_o U_o^2 + \rho_1 g d_o = p_B + \tfrac{1}{2}\rho_o U_{1c}^2 + \rho_1 g (d_{1c} + h) + \Delta_1, \tag{2.3}$$

$$p_A + \tfrac{1}{2}\rho_o U_o^2 + \rho_2 g d_o = p_B + \tfrac{1}{2}\rho_o U_{2c}^2 + \rho_2 g (d_{1c} + h) + \Delta_2, \tag{2.4}$$

where $\Delta_{1,2}$ are energy losses in the lower and upper layers. In addition, the Bernoulli equation in the lower layer through the bottom of the gravity current gives

$$p_C - p_D = \tfrac{1}{2}\rho_o U_o^2. \tag{2.5}$$

Holyer & Huppert (1980) found both energy-conserving solutions as well as dissipative solutions using an energy closure that maximized the dissipation subject to a constant gravity current mass flux. Tan *et al.* (2011) also presented a steady theory for the gravity current front speed in a two-layer ambient, instead closing the problem with an *ad hoc* approximation to the interface displacement over the current, $d_{2c} = (1/2)(H - d_o)$.

The theories for conjugate flows across a horizontal jump discontinuity require an assumption about the form of the energy dissipation. The one-dimensional conjugate form of the DJL equation that has been applied to limiting nonlinear internal waves (Lamb 2000, 2002; Stastna & Lamb 2002; Lamb & Wilkie 2004) assumes energy-conservation, but it can be shown that the DJL equation is also consistent with finite spatially uniform (z-independent) dissipation, and it has been applied in this form to gravity currents in continuous stratification (Ungarish 2006; White & Helfrich 2008). Flynn, Ungarish & Tan (2012), in their study of two-layer gravity currents, the Holyer & Huppert system, assumed vertically uniform dissipation, consistent with the gravity

current theory of White & Helfrich ([2008](#)). They found a relation for the steady front speed that showed reasonable agreement with numerical and experimental results in the limit of large h, but deviated for thin currents, most likely due to the generation of upstream internal waves. Consistent with the theories for gravity currents in continuous stratification, we also apply an assumption of spatially uniform dissipation to the Holyer & Huppert system to find steady solutions which apply in the subcritical and supercritical limits, before treating upstream disturbances in §[3](#).

Assuming uniform dissipation gives $\Delta_1 = \Delta_2 \equiv \Delta$. We have also made some calculations assuming either $\Delta_1 = 0$ or $\Delta_2 = 0$, and the steady gravity current solutions show only very subtle differences. Applying the Bernoulli equation in the ambient lower layer along the gravity current dividing streamline gives an explicit expression for the energy loss:

$$\Delta = (\rho_c - \rho_1)gh - \tfrac{1}{2}\rho_o U_{1c}^2. \tag{2.6}$$

From here on we scale all lengths by H, setting $H = 1$, and scale all velocities by $(g'H)^{1/2}$. Subtracting ([2.4](#)) from ([2.3](#)) and substituting ([2.1](#)) and ([2.2](#)) gives

$$d_o - d_{1c} - h = \frac{1}{2}U_o^2 \left[\frac{d_o^2}{d_{1c}^2} - \frac{(1-d_o)^2}{(1-d_{1c}-h)^2} \right]. \tag{2.7}$$

Further, conservation of momentum, which requires $\int [p(z) + \rho(z)U^2(z)]\,\mathrm{d}z =$ constant through sections 1 and 2, together with the hydrostatic pressure approximation in each section and ([2.5](#)), results in the additional constraint

$$\frac{h^2}{2S} - \frac{h}{S} + \frac{1}{2}d_{1c}^2 - \frac{1}{2}d_o^2 + d_o - d_{1c} + d_{1c}h + U_0^2 \left[-\frac{1}{2} + \frac{d_o^2}{d_{1c}} + \frac{(1-d_o)^2}{1-d_{1c}-h} \right] = 0. \tag{2.8}$$

Equations ([2.7](#)) and ([2.8](#)) are two equations for two unknowns, U_o and d_{1c}, as a function of the current thickness h. These solutions in general do not conserve energy, and the head loss is given by

$$\Delta = \frac{h(1-S)}{S} - \frac{1}{2}U_o^2\frac{d_o^2}{d_{1c}^2}. \tag{2.9}$$

Only solutions with $\Delta \geqslant 0$ are physically relevant, as $\Delta < 0$ implies an external energy source. Energy-conserving gravity currents are important special solutions, and these are found by setting $\Delta = 0$ and solving ([2.7](#))–([2.9](#)) for U_o, h and d_{1c}. The energy-conserving gravity current solutions are identical in the two-layer limit to the conjugate state solutions discussed in White & Helfrich ([2008](#)).

Figure [2](#) shows steady gravity current solutions for a range of d_o and S. In figure [2](#)(*a,b*) energy-conserving solutions are shown for $d_o = 0.1, 0.3, 0.45$. For a given d_o there are two branches, one fast and one slow. It will later be shown that the slow branch is always subcritical with respect to upstream-propagating disturbances, while the other is most often, although not always, supercritical. The slower branch is a single-valued function of S. The faster branch has two energy-conserving solutions for each S up to a critical value, S_c, beyond which these 'supercritical' solutions no longer exist (see also Flynn *et al.* [2012](#)). For $S = S_c$ the curves coalesce, and there is exactly one conjugate state solution. This is consistent with the S_c bound for trapped-core conjugate state solutions in the theory of White & Helfrich ([2008](#)).
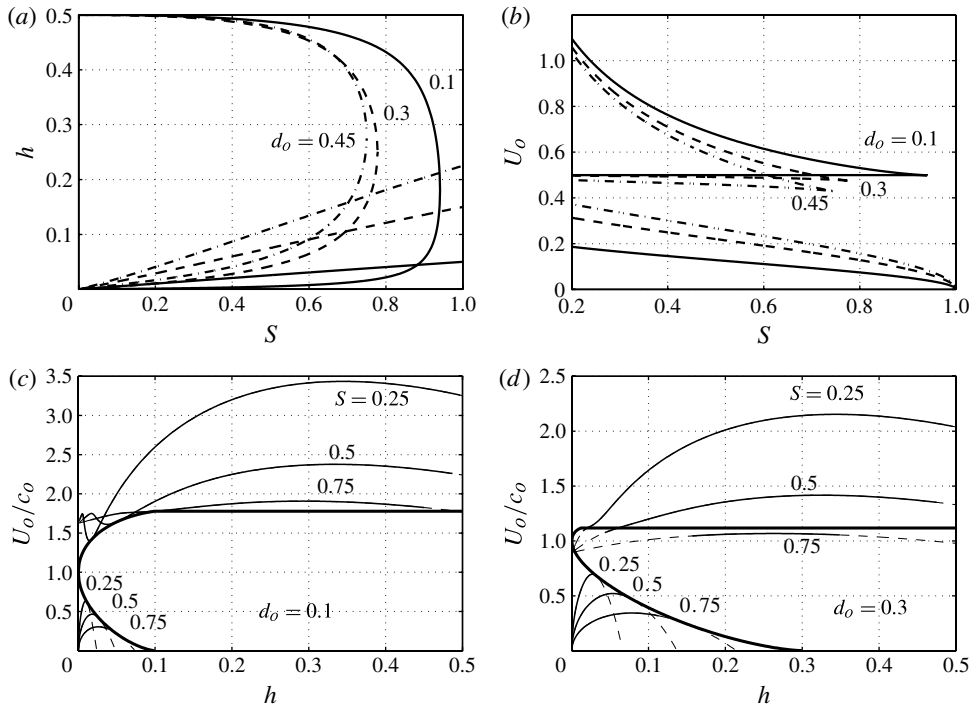
FIGURE 2. Steady gravity current solutions for a range of lower-layer thickness d_o and stratification parameter S. (*a*) Energy-conserving conjugate state solutions for thickness h versus S, and (*b*) conjugate state solutions for front speed U_o versus S: solid lines, $d_o = 0.1$; dashed lines, $d_o = 0.3$; dot-dashed lines, $d_o = 0.45$. Both subcritical and 'supercritical' solution branches are shown. (*c,d*) Front speed versus thickness for (*c*) $d_o = 0.1$ and (*d*) $d_o = 0.3$ for $S = 0.25$, 0.5 and 0.75 (non-physical regions with $\Delta < 0$ shown by dashed lines). Boundary curves for critical flow over topography (2.12) shown by thick lines.

Figures 2(*c*) and 2(*d*) show solutions for $d_o = 0.1$ and $d_o = 0.3$ respectively, for $S = 0.25$, 0.5 and 0.75. Solutions that transition between $\Delta > 0$ (solid lines) and $\Delta < 0$ (dashed lines) are the energy-conserving solutions, and it is apparent that the subcritical branch has only one such transition and the 'supercritical' branch has two. Also shown are the subcritical and supercritical limiting curves for two-layer flow over topography (Baines 1984), which are discussed in the next section.

2.5. *Resonant generation by topography in 2-layer stratification*

We have idealized a gravity current as being equivalent to finite-height topography subject to an additional momentum constraint, such that their behaviour should be governed by the general theory of two-layered hydrostatic flow over topography (Baines 1984). Although this generalized theory does not include the non-hydrostatic effects responsible for solitary waves and undular bores, it can be used as a framework for understanding regimes of gravity current behaviour, including those which generate upstream internal waves, and has the advantage of being fully nonlinear. Baines (1984) used hydraulic theory to describe various regimes including subcritical flow, supercritical flow, blocking, and upstream generation of undular bores and rarefaction waves. Upstream disturbances are generated for parameters (U_o, d_o, h) in which the

linear long-wave speed over the topography is critical,

$$c_l = \frac{U_o}{1-h} + (U_{1c} - U_{2c})\frac{1-h-2d_{1c}}{1-h} - \left[\left(1 - \frac{(U_{1c} - U_{2c})^2}{1-h}\right)\frac{d_{1c}(1-h-d_{1c})}{1-h}\right]^{1/2}$$
$$= 0, \tag{2.10}$$

in the frame translating with the gravity current. Here $U_{1c,2c}$ and $d_{1c,2c}$ are the speeds and thicknesses of the respective layers over the obstacle crest. The bounding curves in (h, U_o) parameter space for critical flow can be found explicitly by solving

$$d_o(1 - d_o)\left(\frac{U_o}{c_o}\right)^2\left[\frac{d_o^2}{d_{1c}^3} + \frac{(1-d_o)^2}{(1-d_{1c}-d_oh)^3}\right] - 1 = 0, \tag{2.11}$$

$$\frac{1}{2}d_o(1 - d_o)\left(\frac{U_o}{c_o}\right)^2\left[\frac{d_o^2}{d_{1c}^2} + \frac{(1-d_o)^2}{(1-d_{1c}-d_oh)^2}\right] + d_{1c} + d_o(h-1) = 0, \tag{2.12}$$

where

$$c_o = \sqrt{d_o(1-d_o)} \tag{2.13}$$

is the linear long-wave speed in the two-layer ambient; see Baines (1995), in which (3.6.7) corresponds to (2.10) and (3.6.5) corresponds to (2.11)–(2.12). In figure 2(c,d), the boundary curves corresponding to the onset of critical flow over topography of height h are shown for $d_o = 0.1$ and 0.3. It can be seen that the slower Holyer–Huppert solution branch always falls below the lower boundary of the critical regime from Baines' theory. The Holyer–Huppert upper branch is for the most part above the bounding supercritical curve, except for $S \to 1$ where these solutions are found below Baines' limit. Note that Baines' supercritical curve is, like the subcritical curve, parabolic for small h, but becomes flat when h is beyond a critical value. Baines (1984) explains that the parabolic branch terminates at a specific h (which depends on d_o) and is met by a spurious branch, so that the supercritical boundary to the right is constant and equal to the value of U_o at the termination point. This value of U_o is very close but not equal to C_{cs} (and also varies slightly with d_o). However, since C_{cs} is the fastest wave supported by the ambient waveguide, and consistent with Stastna & Peltier (2005), we argue that C_{cs} is the appropriate upper limit for critical flow in the flat region and we terminate the upper parabolic curve at $U_o = C_{cs}$. The subtle distinction between C_{cs} and the Baines upper limit is not explored further.

3. Incorporation of an upstream bore into conjugate flow theory

For combinations of (h, U_o) between the subcritical and supercritical boundaries, Baines (1984) showed that the flow over the obstacle crest must be critical, and disturbances will propagate upstream in the form of internal bores, which have been observed in experiments (Baines 1984; Melville & Helfrich 1987). These upstream bores may be undular trains of large-amplitude internal waves due to non-hydrostatic dispersion (Grimshaw & Smyth 1986; Melville & Helfrich 1987) and in the extended KdV model the upstream disturbance can be a monotonic, or conjugate, bore (Melville & Helfrich 1987). Recall that non-hydrostatic effects are included in these models, but are not present in Baines' hydrostatic theory. In the critical flow regime, Baines (1984) introduced an upstream bore connected to the flow near the region of topography. Rottman & Simpson (1989) extended this framework to gravity currents in the

limit $d_o \ll 1$ by treating the current as topography. A schematic of this approach is shown in figure 1(*b*). The region immediately upstream of the current has layer thicknesses $d_{11,21}$ and speeds $U_{11,21}$ in the lower and upper layers, respectively. These are connected to the upstream ambient by a bore which moves with speed C_b in the moving frame. (In the laboratory frame the bore speed is $C_b + U_o$.) Here we extend the approach of Baines (1984) and Rottman & Simpson (1989) to arbitrary d_o by using the gravity current theory described in the previous section together with a jump closure for the upstream bore.

Several models have been proposed for two-layer internal jumps which connect regions of uniform upstream and downstream conditions. Jump conditions must conserve mass and momentum but require an additional assumption about energy dissipation, and several models have been proposed for this closure, with those of Yih & Guha (1955), Chu & Baddour (1977) and Wood & Simpson (1984) cited frequently (see Baines 1995). More recently, Klemp, Rotunno & Skamarock (1997) proposed a jump condition that conserves energy only in the expanding layer, and gives

$$U_o + C_b = \left[\frac{d_{11}^2 (1 - d_{11})(2 - d_{11} - d_o)}{d_{11} + d_o + d_{11}^2 - 3d_o d_{11}} \right]^{1/2}. \tag{3.1}$$

We remind the reader that C_b is the bore speed in the frame moving with U_o and hence $U_o + C_b$ is the bore speed in the laboratory frame.

Klemp *et al.* (1997) showed by comparison with numerical solutions to the Navier–Stokes equations that energy conservation in the expanding layer is a good approximation for flows upstream of the bore with no vertical shear, the case here. This closure reproduces the Benjamin (1968) gravity current front condition in the limit $d_o \to 0$, and is thus preferable to earlier closures. In addition, the Klemp *et al.* solution reproduces the Boussinesq energy-conserving conjugate bore derived by Lamb (2000), $C_b = 0.5$, $d_{11} = 0.5$, independent of d_o. This can be verified from Klemp *et al.*'s relationship for the rate of total energy dissipation (in the frame moving with C_b)

$$D_b = \frac{(U_o + C_b)^3 (1 - d_o)(1 - 2d_{11})(d_{11} - d_o)^3}{2d_{11}^2 (1 - d_{11})^2 (2 - d_{11} - d_o)}. \tag{3.2}$$

The relation (3.2) shows that the conjugate bore, with speed $U_o + C_b = 0.5$, $d_{11} = 0.5$ and $D_b = 0$, is the largest-amplitude bore which is energetically favourable (i.e. $D_b \geqslant 0$). For $d_{11} > 0.5$, the speed decreases and D_b is negative, suggesting that an external energy source is required. This range, as discussed later, is still relevant to the gravity current problem, as the dense front can act as a source of energy to the bore.

The bore closure (3.1) connects the upstream ambient with the region ahead of the gravity current (sections 2 and 3, respectively, from figure 1*b*). In addition, mass conservation between sections 2 and 3 gives

$$(U_{11} + C_b)d_{11} = (U_o + C_b)d_o, \tag{3.3}$$

$$(U_{21} + C_b)(1 - d_{11}) = (U_o + C_b)(1 - d_o). \tag{3.4}$$

The Bernoulli equation is then applied along the dividing ambient streamline between the sections behind and ahead of the gravity current front, 1 and 3 respectively, as

in (2.7) for a steady gravity current, which gives

$$d_{11} - d_{1c} - h = \frac{1}{2}U_{11}^2 \left[\frac{d_{11}^2}{d_{1c}^2} - 1 \right] + \frac{1}{2}U_{21}^2 \left[1 - \frac{(1-d_{11})^2}{(1-d_{1c}-h)^2} \right]. \qquad (3.5)$$

Finally, applying conservation of momentum between sections 1 and 3 (in figure 1a), as in (2.8) for a steady current, yields

$$\frac{h^2}{2S} - \frac{h}{S} + \frac{1}{2}d_{1c}^2 - \frac{1}{2}d_o^2 + d_o - d_{1c} + d_{1c}h + U_{11}^2 \left[\frac{1}{2} + \frac{d_{11}^2}{d_{1c}} - d_{11} \right]$$
$$+ U_{21}^2 \left[\frac{(1-d_{11})^2}{1-d_{1c}-h} + d_{11} - 1 \right] = 0. \qquad (3.6)$$

Equations (3.1) and (3.3)–(3.6) constitute five equations in six unknowns: U_o, C_b, U_{11}, U_{21}, d_{11} and d_{1c}. An additional equation is needed. Baines (1984) showed that for solid topography the critical flow condition (2.10) must be satisfied over the obstacle crest, i.e. the location at which $\mathrm{d}h(x)/\mathrm{d}x = 0$, where $h(x)$ is the obstacle boundary. It is tempting to apply this constraint here to close the system, but because the gravity current is a free boundary, the hydraulic control point where $\mathrm{d}h/\mathrm{d}x = 0$ may not correspond to the uniform gravity current region. Rottman & Simpson (1989), rather than using the critical flow condition, imposed energy conservation along the streamline separating the gravity current from the ambient. Analogous to (2.9) for steady currents, the head loss across the current front is

$$\Delta = \frac{h(1-S)}{S} - \frac{1}{2}U_{11}^2 \frac{d_{11}^2}{d_{1c}^2}, \qquad (3.7)$$

and there is a corresponding rate of energy dissipation,

$$D_c = U_o \Delta = U_o \frac{h(1-S)}{S} - \frac{1}{2}U_o U_{11}^2 \frac{d_{11}^2}{d_{1c}^2}. \qquad (3.8)$$

Setting $D_c = 0$ provides a final constraint.

However, to explore the sensitivity of the gravity current/bore solutions (3.1)–(3.6) to dissipation, we systematically vary the dissipation, D_c, and plot corresponding solutions for (h, U_o). These are shown in figure 3 for $d_o = 0.1$ and $d_o = 0.3$ over a range of S values. Solutions are shown only for $\Delta \geqslant 0$, and it can be seen that the solutions take the form of a wedge within the critical flow envelope. For a given h, an increase in gravity current front speed, U_o, corresponds to an increase in bore amplitude d_{11}. The energy-conserving solution ($\Delta = 0$) forms a rightward boundary in (h, U_o), with dissipative solutions to the left. For $d_o = 0.1$ (figure 3a), solutions are found up to the supercritical boundary, and the maximum amplitude is smaller than the conjugate bore $d_{11} < 0.5$. For $d_o = 0.3$ (figure 3b), solutions terminate within the critical flow envelope.

The wedge-shaped region in which the bore solutions exist can be interpreted as the resonant band. In figure 3(c,d) the wedges are shown for various values of S. It can be seen that for a given value of h, there is a larger resonant band in U_o for $d_o = 0.1$ as compared with $d_o = 0.3$. This suggests that a thinner bottom layer is more favourable for resonance.

In some cases the wedge in which bore solutions are found extends to the supercritical boundary (e.g. $d_o = 0.1$, $S = 0.75$, figure 3a). Otherwise the bore solutions terminate when the flow becomes critical through the bore region upstream of the
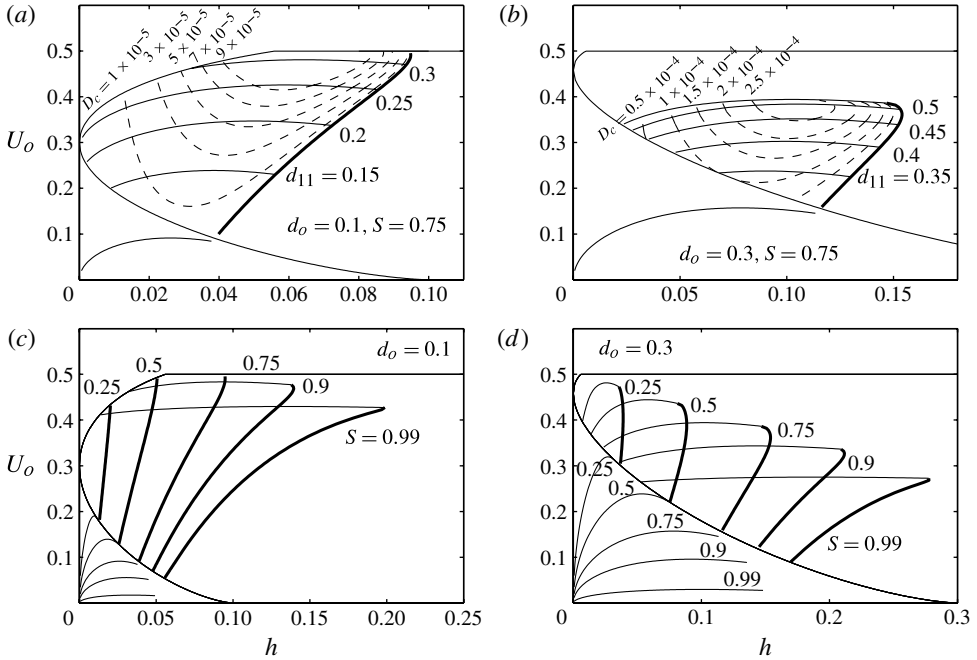
FIGURE 3. (*a,b*) Gravity current solutions with an upstream-propagating bore, for (*a*) $d_o = 0.1$, $S = 0.75$ and (*b*) $d_o = 0.3$, $S = 0.75$. Contours of constant bore amplitude d_{11} (solid lines) and gravity current front dissipation D_c (dashed lines). The energy-conserving ($D_c = 0$) curve is shown in bold. The subcritical solution curve, and sub- and supercritical boundaries from Baines (1984) are also shown as in figure 2 (only where $D_c \geqslant 0$). (*c,d*) Bounding curves for solutions with upstream bores for (*c*) $d_o = 0.1$ and (*d*) $d_o = 0.3$, for $S = 0.25$, 0.5, 0.75, 0.9 and 0.99. The thick line again indicates the $D_c = 0$ curve.

gravity current front, such that

$$c_l = U_o + (U_{11} - U_{21})(1 - 2d_{11}) - [(1 - (U_{11} - U_{21})^2)d_{11}(1 - d_{11})]^{1/2} = 0 \quad (3.9)$$

(e.g. $d_o = 0.3$, $S = 0.75$, figure 3*b*). This limit is analogous to the transition to critical flow immediately in front of solid topography, which was shown by Baines (1984) to correspond to the maximum possible upstream disturbance. Baines showed that beyond this transition (corresponding to his region 4*E*) upstream rarefactions were produced. Lawrence (1993) also experimentally studied this region, which he termed approach control, and also observed rarefactions. Thus beyond the resonant wedge, but within the critical flow region, rarefactions can be expected. Our numerical simulations, discussed in § 4, demonstrate this behaviour, and the details of the rarefactions are discussed in that section. For now we remark that the upper limit to the bore solutions, and the transition to rarefactions, is sensitive to the bore jump condition. Since the Klemp *et al.* condition produces the correct upper bound, it is preferred to that used in Rottman & Simpson (1989), which does not predict an upper bound on the bore amplitude.

The results of the theory, shown in figure 3(*a,b*), suggest that solutions are sensitive to D_c, the gravity current dissipation. For a given current thickness h, allowing a small change in D_c will significantly change the solution, i.e. U_o, d_{11}, C_b. However,
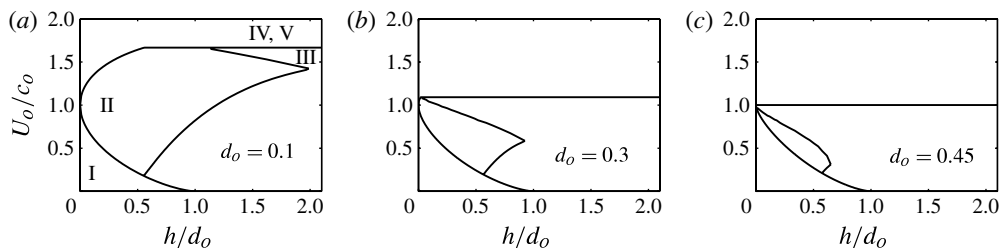
FIGURE 4. Regime diagrams summarizing the hydraulic theories, $Fr = U_o/c_o$ versus h/d_o, for (*a*) $d_o = 0.1$, (*b*) $d_o = 0.3$ and (*c*) $d_o = 0.45$.

the results of numerical simulations, discussed in §4, suggest that the gravity current dissipation is small compared with the energy transferred to the upstream bore, and we find that the solution for $D_c = 0$ compares favourably with numerical results.

3.1. *Summary of hydraulic theories*

Given the complexity of the theories just presented, we summarize them here while drawing comparison to Baines' topographic theory. For reference see figure 4, which shows regions of behaviour in $h - Fr$ space, where $Fr = U_o/c_o$ is the Froude number. Within region I, gravity currents are subcritical and the front speed $U_o(h)$ is given by the lower branch of solutions given by solving (2.7) and (2.8). This corresponds to Baines' region 1*A*. The upper limit for subcritical solutions is given by the lower solution branch of (2.12). In region II, there is an upstream bore and solutions for U_o and C_b are obtained by solving (3.1) and (3.3)–(3.6) as a function of h and the frontal dissipation D_c. This region corresponds to Baines' region 3*C* (and also includes his region 4*C* where $d_{11} > 0.5$). Setting $D_c = 0$ provides the energy-conserving solution. The upper limit for region II is given either by supercritical flow (see below) or where the flow becomes critical through the bore (3.9). Beyond this point, in region III, a rarefaction links the leading conjugate bore to the gravity current front. This corresponds to Baines' region 4*E*. The transition to supercritical flow is given by the upper branch of (2.12) or the limit $U_o = C_{cs}$. In the supercritical region, IV–V, solutions for $U_o(h)$ are given by the upper solution branch of (2.7) and (2.8). This region corresponds to Baines' region 2*B*.

Figure 4 allows direct comparison with the familiar regime diagrams for two-layer topographic flow first developed in Baines (1984, figure 8 for example). The regions of subcritical and supercritical flow and the generation of upstream bores are quite similar for gravity currents and solid topography. As with topography, the size of region II, the resonant band, decreases with increasing d_o. Note that for gravity currents there is no possibility of blocking, which can occur for solid topography. In addition, the Baines theory relies on a different closure for upstream bores (see also Klemp *et al.* 1997). A third difference is that the connection between the gravity current and the bore, as discussed, uses an energy conservation condition for the gravity current (3.8), rather than the critical flow condition (2.10) as for topography.

4. Numerical simulations

To provide a comparison with the steady gravity current theory, two-dimensional numerical simulations were performed for a large parameter range in S, d_o, and reservoir height, h_d.

4.1. *Numerical method*

We solve the two-dimensional Boussinesq–Euler equations,

$$\frac{\mathrm{D}\boldsymbol{u}}{\mathrm{D}t} = -\boldsymbol{\nabla}p - b\hat{\boldsymbol{k}}, \quad \boldsymbol{\nabla} \cdot \boldsymbol{u} = 0, \quad \frac{\mathrm{D}b}{\mathrm{D}t} = 0, \quad \frac{\mathrm{D}}{\mathrm{D}t} = \frac{\partial}{\partial t} + \boldsymbol{u} \cdot \boldsymbol{\nabla}, \qquad (4.1)$$

where p is the pressure (less the hydrostatic component from ρ_2), $b = (\rho - \rho_2)/\Delta\rho$ is the dimensionless buoyancy, and $\hat{\boldsymbol{k}}$ is the unit vector in the positive z-direction. Velocities are scaled by $\sqrt{g'H}$, lengths by H, and time by $H/\sqrt{g'H}$.

The numerical model employs a second-order projection method based on that of Bell & Marcus (1992). The method uses a Godunov-type evaluation of the nonlinear terms (a non-oscillatory finite volume formulation) and is ideally suited to gravity current flows where sharp gradients of density and velocity naturally develop. The Euler equations (4.1) are solved with no explicit dissipation or diffusivity, but the numerical method does introduce some numerical dissipation. However, an important property of the advection scheme is that the numerical diffusion is significant only where large gradients (e.g. shocks) occur on the grid scale. This numerical method has been used successfully for studies of large-amplitude internal solitary waves (cf. Lamb 2002) and tests of the code show that large internal solitary waves can propagate distances of $\sim 100H$ with the correct phase speed, form, and minimal loss of energy ($<1\%$). The scheme was also used in White & Helfrich (2008) for gravity current simulations, where it was found that the front propagation speed compared favourably with experiments, such as those of Maxworthy *et al.* (2002). In addition, calculations have been done with both a small uniform viscosity and a Smagorinsky LES closure, and very little dependence of gravity current properties on the dissipation scheme are observed.

Most of the calculations were carried out in a rectangular domain with length $L = 64$ and height $H = 1$, and a resolution ($x \times z$) of 2048×256. A few were done in a domain with length $L = 50$ and resolution 3000×150. All boundary conditions were free-slip. Each run was started from a stagnant, $\boldsymbol{u} = 0$, dam-break initial condition, with a lock of height h_d and length L_d, and the initial buoyancy field given by

$$b(x, z, t = 0) = \begin{cases} 1/S & z \leqslant h_d, x \leqslant L_d, \\ 1 & h_d < z \leqslant d_o, x \leqslant L_d, \\ 0 & d_o < z \leqslant 1, x \leqslant L_d, \\ 1 & z \leqslant d_o, x > L_d, \\ 0 & d_o < z \leqslant 1, x > L_d. \end{cases} \qquad (4.2)$$

In all cases L_d was sufficiently long that the finite size of the reservoir did not influence the gravity current.

4.2. *Results and classification of regimes*

We have conducted over 200 simulations, varying h_d, S, and d_o in order to explore the full range of behaviour and validate the regimes suggested by the steady theory. Results of the numerical simulations are shown in figures 5–9, which show buoyancy fields at various times, and the position of the gravity current and leading wave fronts with time. From these results, we have classified five characteristic behaviours.

(i) Type I is classified as a subcritical gravity current front. In this case, a localized disturbance is generated around the gravity current front, but there is no appreciable upstream disturbance. The gravity current front typically exhibits
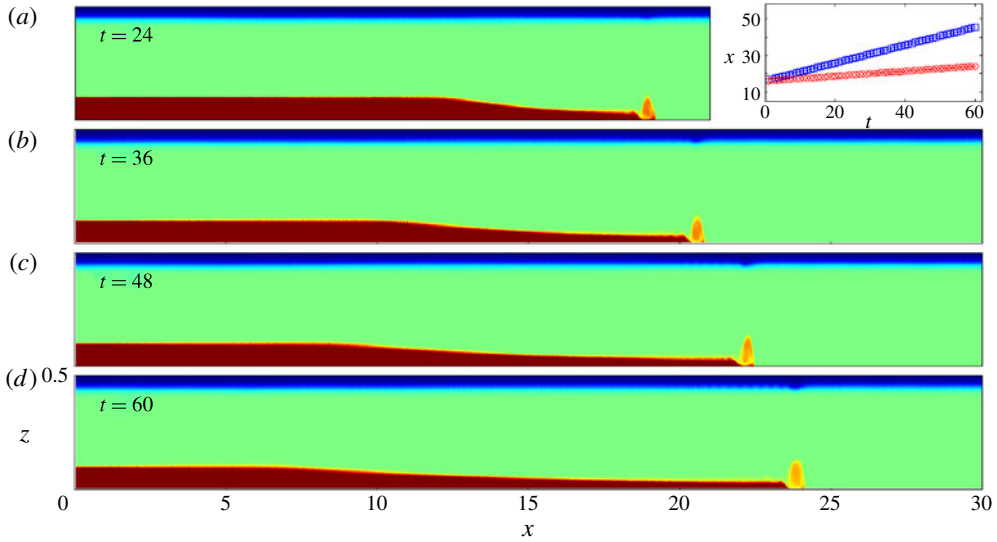
FIGURE 5. Type I behaviour, subcritical front: $d_o = 0.45$, $S = 0.75$ and $h_d = 0.1$. Buoyancy field at (a) $t = 24$, (b) $t = 36$, (c) $t = 48$ and (d) $t = 60$. Upper right inset: position of wave front (blue squares) and gravity current front (red circles).
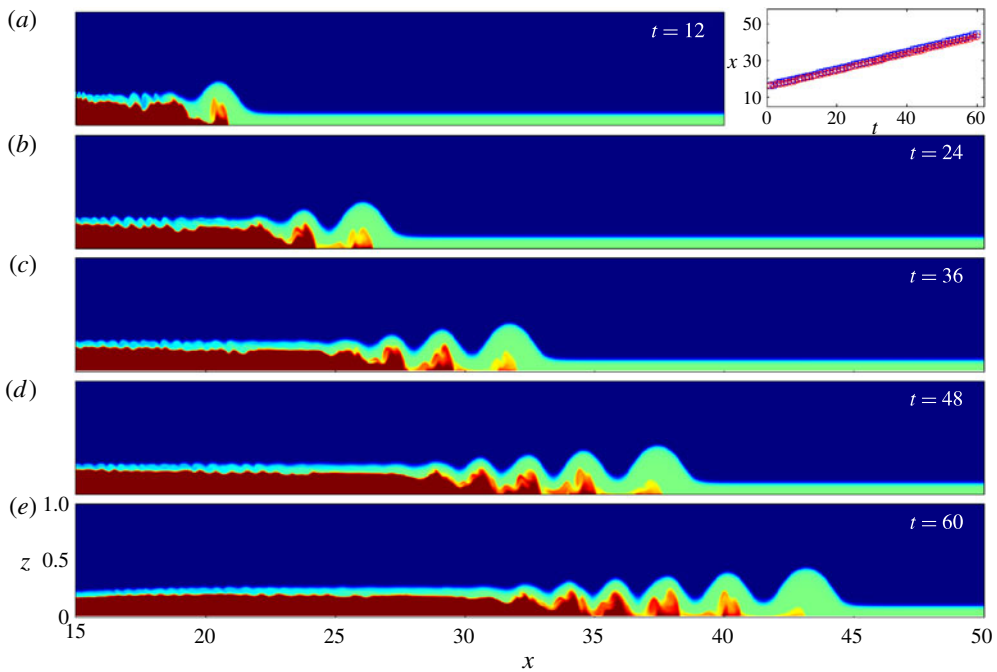

FIGURE 6. Type II behaviour, with resonant generation of nonlinear internal waves: $d_o = 0.1$, $S = 0.9$ and $h_d = 0.45$. Buoyancy field at (a) $t = 12$, (b) $t = 24$, (c) $t = 36$, (d) $t = 48$ and (e) $t = 60$. Upper right inset: position of wave front (blue squares) and gravity current front (red circles).
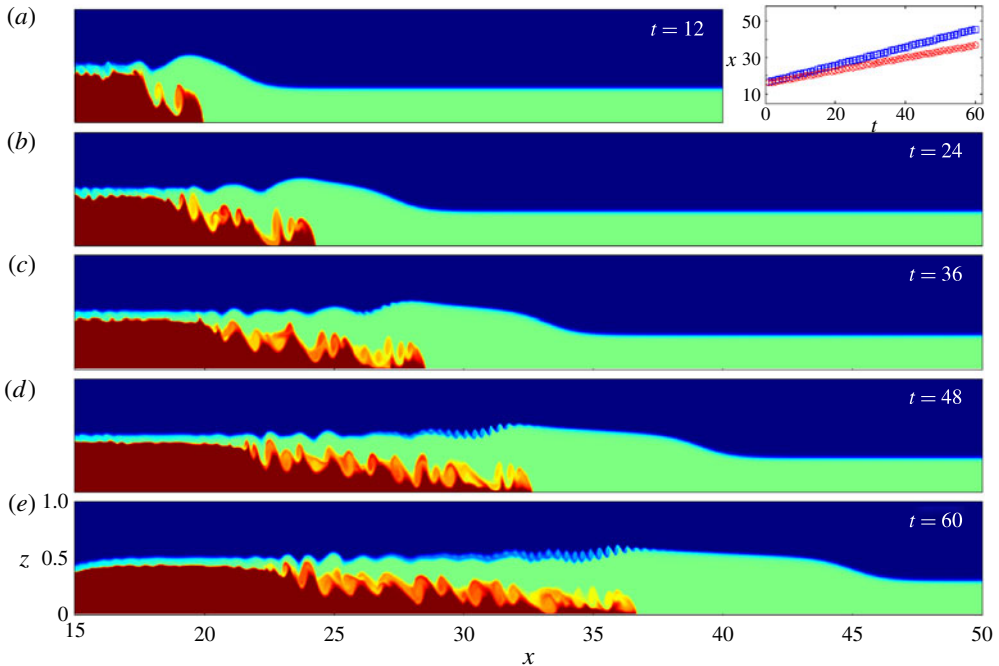
FIGURE 7. Type III behaviour, with upstream rarefaction wave: $d_o = 0.3$, $S = 0.9$ and $h_d = 0.7$. Buoyancy field at (a) $t = 12$, (b) $t = 24$, (c) $t = 36$, (d) $t = 48$ and (e) $t = 60$. Upper right inset: position of wave front (blue squares) and gravity current front (red circles).

a distinct bump, sometimes called a head wave. The dividing ambient streamline exhibits a depression immediately above the bump, travelling at the same speed as the front (see figure 5). In this regard, this regime is very similar to subcritical flow over a solid topographic bump (Long 1954; Baines 1984). Note that in figure 5 the leading wave, with very small amplitude, travels at a speed close to the linear long wave speed $c_o = \sqrt{d_o(1 - d_o)}$ and is outside the region shown in the figure. This is consistent with hydraulic theory, which predicts a transient disturbance with speed c_o following the introduction of a bump at $t = 0$ for a subcritical flow.

(ii) The Type II regime exhibits resonant generation of nonlinear internal waves (figure 6). The disturbance takes the form of an undular bore, which moves upstream at a speed faster than the gravity current front. The gravity current front itself develops wave-like oscillations, and for larger disturbances, dense gravity current fluid periodically detaches and propagates upstream with the leading waves. It is important to note that these waves are not generated with the initial dam break collapse, but are continuously initiated at the front, undergoing a growth sequence that begins with the wave locked to the front, growing in amplitude and increasing in speed, before finally detaching when its speed exceeds the speed of the gravity current. This can be seen in figure 6 ($d_o = 0.1$, $S = 0.9$, $h_d = 0.45$), where the number of waves evolves from one at $t = 12$ to as many as six by $t = 60$. This process is consistent with a resonance whereby energy is transferred from the front to the waves. Note that the case shown is an example of a large-amplitude bore, and the gravity current fluid detaches and is
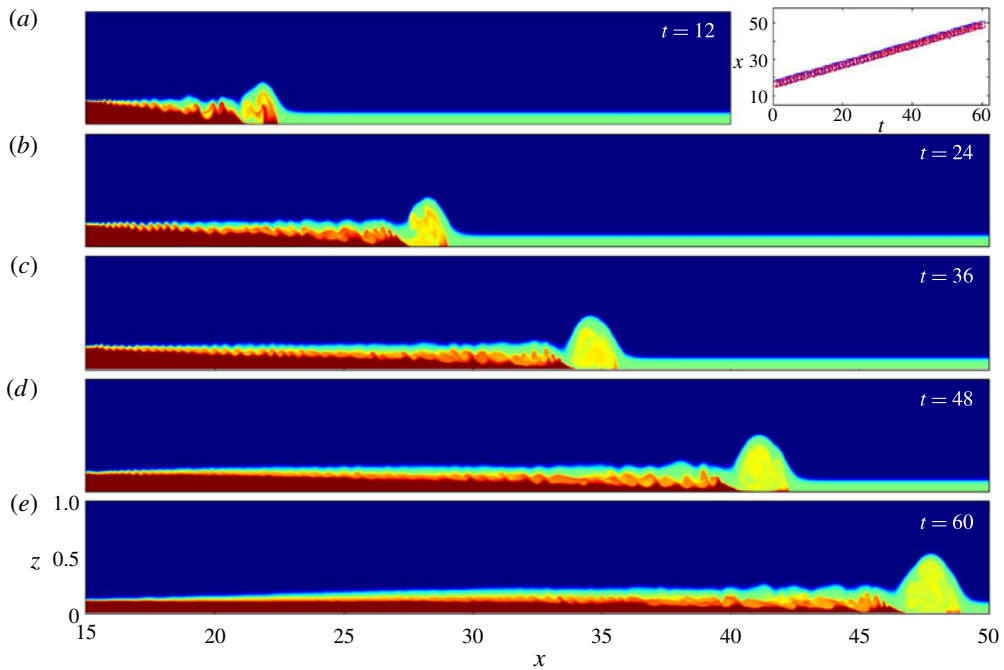
FIGURE 8. Type IV behaviour, with a single trapped wave at the front: $d_o = 0.1$, $S = 0.5$ and $h_d = 0.35$. Buoyancy field at (*a*) $t = 12$, (*b*) $t = 24$, (*c*) $t = 36$, (*d*) $t = 48$ and (*e*) $t = 60$. Upper right inset: position of wave front (blue squares) and gravity current front (red circles).
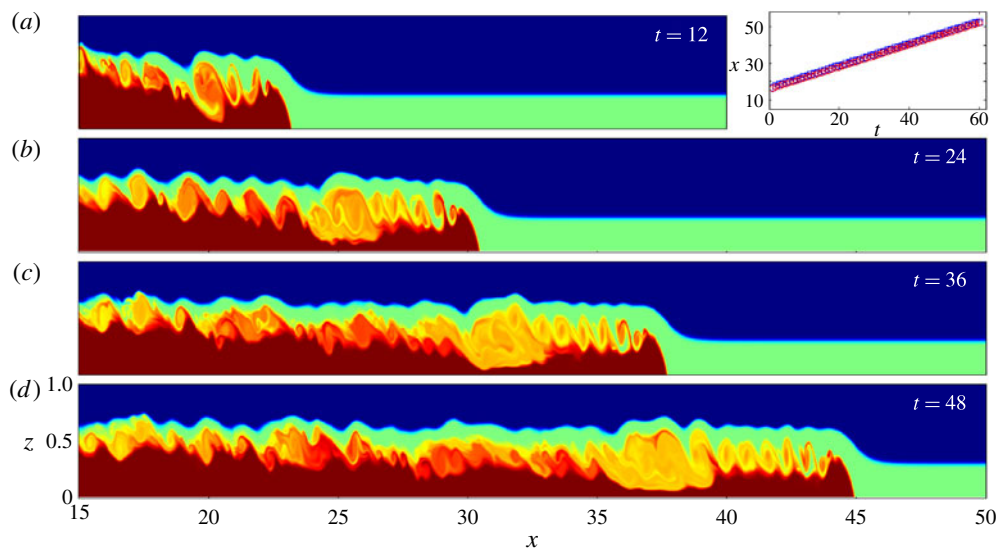

FIGURE 9. Type V behaviour, supercritical gravity current: $d_o = 0.3$, $S = 0.5$ and $h_d = 0.95$. Buoyancy field at (*a*) $t = 12$, (*b*) $t = 24$, (*c*) $3t = 6$ and (*d*) $t = 48$. Upper right inset: position of wave front (blue squares) and gravity current front (red circles).

carried in the core of the waves. In this case the speed of the gravity current front and the leading bore are nearly equal. This condition is the most favourable for resonance.

(iii) The Type III regime exhibits an upstream monotonic bore connected to the gravity current front by an expanding rarefaction. The rarefaction connects the faster-moving bore to the slower gravity current front. Baines (1984) observed a very similar regime in two-layer topographic flow, which can be explained in terms of the bore characteristics. The conjugate bore found by Lamb (2002) and also in the Klemp *et al.* closure (3.1) is the largest-amplitude bore that is energetically favourable. Beyond the conjugate bore, an increase in amplitude corresponds to decreasing bore speed (from (3.1)), suggesting that an expanding rarefaction wave will connect the leading conjugate bore to the region near the gravity current front. The Type III simulations, for example $d_o = 0.3$, $S = 0.9$ and $h_d = 0.7$, shown in figure 7, illustrate this phenomenon.

(iv) The Type IV regime exhibits an interesting, single large-amplitude solitary wave-like disturbance that is locked to the gravity current front. An example is shown for $d_o = 0.1$, $S = 0.5$, $h_d = 0.35$ in figure 8. In this regime, the speed of the disturbance and the current front are in the supercritical region of (h, U_o) space. This is consistent with their increased speed relative to, for example, Type III waves. Over the duration of the numerical solution the disturbance is not quite steady, and grows slowly by entraining dense fluid from the gravity current into a recirculating, turbulent core. We note that after an initial development period, the speed and amplitude of both the leading disturbance and the gravity current front remain approximately constant until the end of the simulation time.

(v) Type V is classified as a supercritical gravity current. This case is the limit in which there is a uniform current thickness (on average) behind the front, and the displacement of the ambient interface is uniform and monotonic over the current front. For these cases, the flow over the front is smooth, but there is substantial turbulent mixing behind the front, as is typical of gravity currents. It should be noted that the numerical simulations are two-dimensional and these Kelvin–Helmholtz structures (which are also evident behind the rarefaction wave in the Type III simulation in figure 7) would break down in three-dimensional turbulence. As a result, while the gravity current and wave fronts are accurately captured, the model does not resolve the characteristics of the mixing behind the fronts.

Later we will show that in the limit of $h_d \to 1$, Type V gravity currents approach the energy-conserving conjugate states from Holyer & Huppert (1980) and White & Helfrich (2008) (shown in figure 2a,b). We also note that, with the exception of the Type IV response, the disturbances to the ambient stratification discussed above have direct analogues in the problem of transcritical stratified flow over topography where upstream propagating undular and monotonic bores, along with both localized subcritical and supercritical responses over the topography have been found in extended-KdV models (Melville & Helfrich 1987; Grimshaw *et al.* 2002), laboratory experiments (Melville & Helfrich 1987) and full Navier–Stokes numerical solutions (Stastna & Peltier 2005).

5. Gravity current properties

In order to quantitatively compare the gravity current theory with the numerical simulations, the gravity current speed U_o and thickness h, as well as the characteristics

of the upstream bores, were extracted from the results. Note that while the numerical simulations varied the lock height h_d, the current thickness, h, is part of the solution and must be determined *a posteriori*. In an ideal three-layer system, the current thickness would be defined by the contour of $b = 1/S$ (the non-dimensional gravity current buoyancy). However, because the simulations are turbulent, this contour is highly irregular and an integral measure is preferable. For example, Marino, Thomas & Linden (2005, see their (3.1)) give an estimate of the thickness of gravity current based on the equivalent hydrostatic pressure. We adapt the concept of an integral measure, but instead estimate the thickness, $h(x, t)$, based on the potential energy of the gravity current. Behind the front, the available potential energy relative to the upstream ambient, up to the level z^* at which $\rho(x, z^*) = \rho_1$, is

$$PE^* = \int_0^{z^*} (\rho(x, z, t) - \rho_1) gz \, \mathrm{d}z \qquad (5.1)$$

(see e.g. Cheong, Kuenen & Linden 2006). In an ideal, sharp three-layer system, $z^* = h(x, t)$, and the excess potential energy would be

$$PE^* = \tfrac{1}{2}(\rho_c - \rho_1) h(x, t)^2. \qquad (5.2)$$

Setting these expressions equal defines $h(x, t)$.

The gravity current front, x_f, is defined as the most forward point at which $h(x) > 0.005$ (a reasonable threshold value). The front speed, U_o, can then be calculated by linear regression of x_f versus t over the duration of the simulation. The regressions are highly linear, as seen in figures 5–9, with $R^2 > 0.999$ in most cases.

Because there is considerable variability in $h(x, t)$ (in space, time and, particularly, between regimes), we define two measures of the mean gravity current thickness. The first, h_o, is the largest local maximum of $h(x)$ within the region two units behind the front: $\max(h(x))$, $x_f - 2 \leqslant x \leqslant x_f$. This definition captures the very distinct maximum immediately behind the front in the Type I, Type IV and, to some extent, Type V cases (see figure 10a,b). However, by using a two-unit window behind the front, smaller maxima near x_f, which occur in the oscillatory Type II cases, are rejected (see figure 11a). A second measure, $\bar{h}$, is defined as the average of h over the region two units behind the first local maximum (see figures 10–11). To get a single value for both h_o and $\bar{h}$ for each simulation, a time average is taken for each one between $t = 30$ and the final state, $t = 60$. It was found that $t = 30$ was sufficient for the average current thickness near the front to stabilize following the initial dam break.

The characteristics of the upstream disturbances have also been measured. First, the amplitude of the upstream bore, d_{11}, is measured as the mean height of the $b = 0.5$ contour over the region from the gravity current head (where $h(x) = h_o$) forward to the point at which its displacement is midway between d_o and its first maximum (see figure 11). This averages over the upstream waves. The wave amplitudes are of interest, but are not discussed since the focus is on the properties of the gravity current. However, in the weakly nonlinear KdV model the amplitude of the leading wave in an undular bore is twice the bore amplitude $d_{11} - d_0$ (see Whitham 1974). Esler & Pearce (2011) have studied the development and properties of two-layer undular bores using an extension of the modulation theory of Whitham (1974) applied to a fully nonlinear, weakly dispersive internal wave model.

In §7, the energy exchange between the gravity current and the bore is analysed. For this purpose we take a control volume between the undisturbed upstream ambient
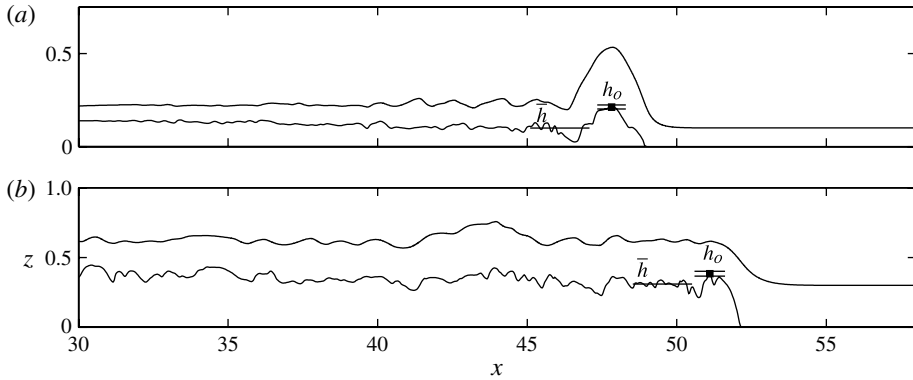
FIGURE 10. Estimates of gravity current thickness: h_o is the head height, defined at the first maximum behind the front (square, with error bars), and $\bar{h}$ is the average height behind the first maximum (horizontal line). Contours of gravity current thickness, $h(x, t)$, and $b = 0.5$ for (*a*) $d_o = 0.1$, $S = 0.5$, $h = 0.35$ (Type IV) and (*b*) $d_o = 0.3$, $S = 0.5$ and $h = 0.95$ (Type V).
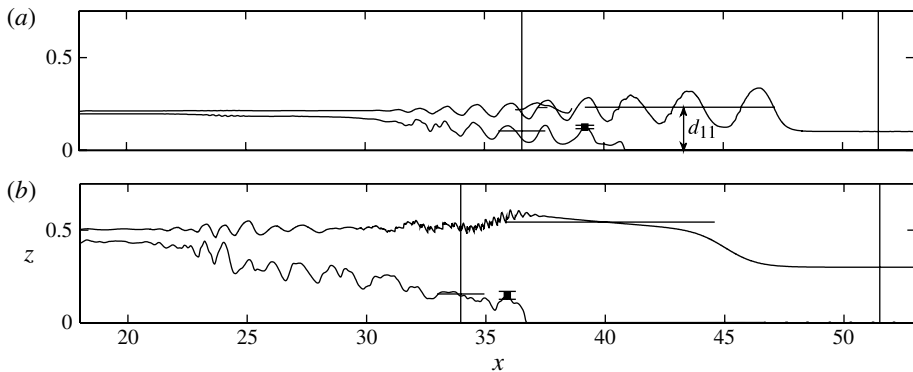

FIGURE 11. Upstream bore characteristics for (*a*) $d_o = 0.1$, $S = 0.9$ and $h_d = 0.35$ (Type II) and (*b*) $d_o = 0.3$, $S = 0.9$ and $h_d = 0.7$ (Type III). Average height, d_{11}, taken through the region between the gravity current head and the point where the $b = 0.5$ contour is midway between d_o and its first maximum. Vertical lines show the regions in the upstream ambient and behind the head where energy fluxes are calculated. Estimates for h_o and $\bar{h}$ also shown, as in figure 10.

and the uniform region behind the gravity current head. The boundaries of the control volume are shown in the vertical lines in figure 11. In addition, the speed of the upstream bore, C_w, is calculated by linear regression of x_w versus t, where x_w is the point at which the $b = 0.5$ contour exceeds a threshold value (5 % of the maximum displacement). From figures 5–9 it can be seen that the regression is highly linear, and the uncertainty in C_w, like U_o, is very small (generally less than 1 % of their mean value). The uncertainties in h_o and $\bar{h}$ are substantially higher, particularly for the oscillatory Type II cases, but usually less than 10 % of their mean.
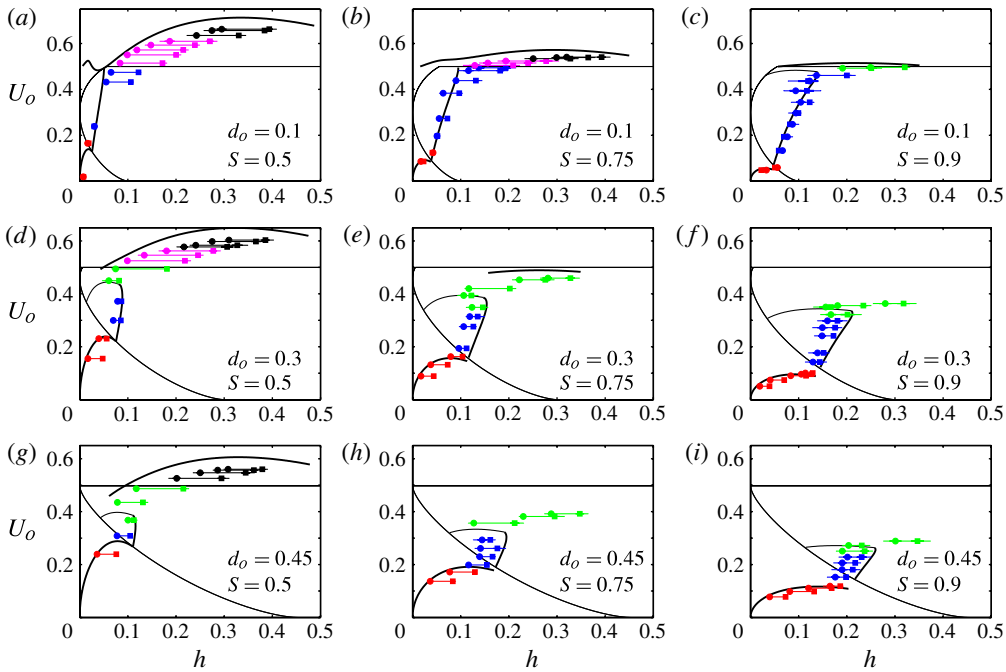
FIGURE 12. Gravity current solutions U_o versus h for a range of layer depth d_o and stratification parameter S: (a–c) $d_o = 0.1$, (d–f) $d_o = 0.3$, (g–i) $d_o = 0.45$; (a,d,g) $S = 0.5$, (b,e,h) $S = 0.75$, (c,f,i) $S = 0.9$. Subcritical and supercritical gravity current solutions shown by thick lines. Boundary curves for critical flow over topography (2.12) shown by thin black lines. The resonant wedge in which gravity current/bore solutions exist is also shown, where the rightmost thick curve represents the energy-conserving solution ($\Delta = 0$). Symbols show numerical results: Type I (red), Type II (blue), Type III (green), Type IV (magenta), and Type V (black). The two estimates for current thickness are also shown, $\bar{h}$ (circles) and h_o (squares). Error bars in U_o, h_o, and $\bar{h}$ are shown for each point (the uncertainty range in U_o is smaller than the symbol size).

6. Comparison of simulations with hydraulic theory

6.1. *Gravity current front speed versus thickness*

Having extracted measures of h and U_o from the simulations, we can compare the results with the hydraulic theory of §§ 2 and 3. In figure 12, predictions of the steady theory are shown for $d_o = 0.1$, 0.3 and 0.45 for $S = 0.5$, 0.75 and 0.9 along with the numerical results (U_o, h, and regime type). The boundaries of the critical flow region from (2.12) are shown along with both the subcritical and 'supercritical' branches of the gravity current solutions for each (d_o, S) combination. Note that only energetically favourable solutions ($\Delta \geqslant 0$) are shown. The fast branch is not strictly supercritical, sometimes falling partially (or completely) within the critical flow region, and occupying more of the critical flow region as d_o and S increase. This is expected, since as $d_o \to 0$ or $S \to 0$ the Benjamin gravity current limit is approached, for which there are no upstream disturbances.

First, consider the subcritical regime, for which the numerical results compare quite favourably with the theory. We plot both h_o and $\bar{h}$ (in addition to horizontal error bars for each) in order to convey the variability in the numerical current thickness (which

is of course assumed constant in the theory). For all d_o, S combinations, the theory captures both the U_o versus h behaviour as well as the region in (h, U_o) space in which subcritical, Type I behaviour is observed in the simulations. The front speed, U_o, initially increases for small h before reaching a local maximum, very close to the lower critical boundary curve. The numerical results follow the subcritical curve and approach the local maximum in U_o predicted by theory just before the transition to critical flow.

The hydraulic theory predicts a transition to Type II behaviour (upstream-propagating internal waves/bores) where $U_o(h)$ exceeds the lower critical flow boundary. This transition from Type I to Type II behaviour in the numerical results is captured quite well by the theoretical bounds. There is some 'fuzziness' of the boundary for a few cases, but in general the transition is quite robust for all (d_o, S). Within the critical flow region, the Type II numerical results nearly always fall within the resonant wedge predicted by the theory of § 3, even allowing for the variability between h_o and $\overline{h}$ (which can be significant for Type II cases). In addition, the numerical results show very good agreement with the theoretical zero dissipation curve (the rightmost boundary curve of the resonant wedge). See in particular $d_o = 0.1$, $S = 0.75$ and $S = 0.9$ (figure 12b,c). In general, the size of the resonant wedge increases for smaller d_o and larger S, meaning a larger range of parameter space generates upstream disturbances.

Within the resonant wedge, the theory predicts undular bores up to a limiting amplitude. This maximum amplitude may be larger than the conjugate bore, $d_{11} = 0.5$, as we discuss further in § 7. This is true in particular for $d_o = 0.45$, where the majority of the bore solutions have $d_{11} > 0.5$. Outside region II (where the transition is due to the onset of critical flow through the bore region), there is a rarefaction connecting the gravity current front to the faster maximum-amplitude bore. The numerical simulations clearly demonstrate this Type III behaviour. For the most part, Type III rarefactions lie between the resonant wedge and the upper limit for critical flow (the conjugate bore speed, $C_{cs} = 0.5$).

Where $U_o > C_{cs}$, the gravity current front speed is supercritical and rarefactions are no longer observed. Rather, we see Type IV (single forced waves) and Type V (conjugate gravity currents) supercritical behaviour. For these cases, the numerical gravity current front speed always equals that of the leading wave, $U_o = C_w$, consistent with critical flow theory. For most d_o, S combinations there is a fast gravity current solution branch that is, for the most part, supercritical. Examples are $d_o = 0.1$, $S = 0.5$ (figure 12a), $d_o = 0.1$, $S = 0.75$ (figure 12b) and $d_o = 0.3$, $S = 0.5$ (figure 12d). There is reasonably good qualitative agreement between the steady supercritical solutions for U_o versus h and the numerical results. However, the numerical results consistently fall below the theoretical curve in each of these cases. The reason is not immediately clear, but there is considerable spread in the estimates of gravity current thickness for these cases, which contributes uncertainty to the comparison. There is also a small amount of numerical dissipation.

For two cases, $d_o = 0.1$, $S = 0.9$ (figure 12c) and $d_o = 0.3$, $S = 0.75$ (figure 12e), the faster gravity current solution branch falls completely within the critical flow region. In this region, since $U_o < C_{cs}$, theory would predict an upstream conjugate bore with a rarefaction, which the occurrence of Type III simulation results confirm. Nonetheless, the steady gravity current solution (neglecting an upstream disturbance) still predicts the U_o versus h behaviour of these Type III gravity currents quite well, in fact arguably better than comparison between the supercritical curves and the Type IV and V curves. This suggests that, at least for these two cases, the upstream wave does
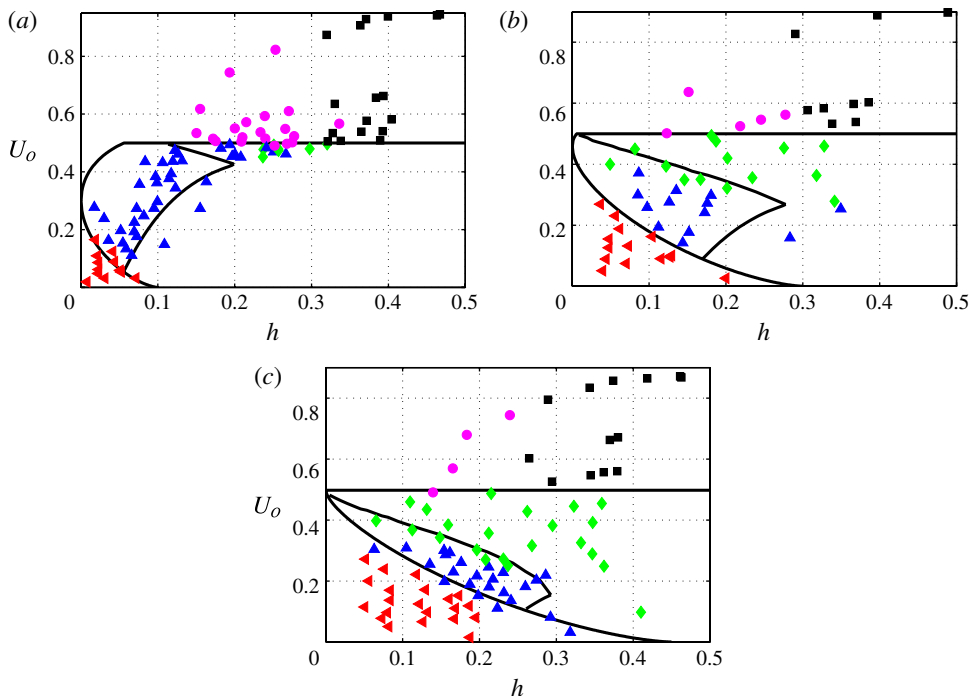
FIGURE 13. Regime diagrams in (h, U_o) for (*a*) $d_o = 0.1$, (*b*) $d_o = 0.3$ and (*c*) $d_o = 0.45$; only h_o (not $\bar{h}$) is shown for visual clarity. Symbols: $\triangleleft$, Type I; $\triangle$, Type II; $\diamond$, Type III; $\bigcirc$, Type IV; $\square$, Type V.

not substantially affect the gravity current front. For these two cases, U_o is just below $C_{cs} = 0.5$, suggesting the upstream disturbance is only slightly faster than the gravity current front, and the upstream energy transfer is weak. We comment further on this issue in §7.

For some combinations of (d_o, S), the fast gravity current branch ceases to exist. See for example figure 12(*f*) ($d_o = 0.3$, $S = 0.9$), figure 12(*h*) ($d_o = 0.45$, $S = 0.75$), and figure 12(*i*) ($d_o = 0.45$, $S = 0.9$). As shown in figure 3 and discussed in §2.4, for $S > S_c$ (for a given d_o), there are no energetically favourable gravity current solutions, but instead only an upstream conjugate bore is expected. Indeed the numerical results corresponding to these cases show a Type III conjugate bore with rarefaction. However, a prediction for the upper U_o limit is not available for these cases.

6.2. *Regime diagrams*

From the union of the resonant wedges for all *S*, a regime diagram can be constructed for each d_o in (h, U_o) space. These are shown in figure 13. As before, boundaries from (2.12) separate subcritical, supercritical, and critical flow regions, and the boundaries of the gravity current/bore solutions form an additional region, in which upstream undular bores can be expected (Type II). Outside this region, rarefactions are expected (Type III). The numerical results are plotted with these bounding curves. These regions describe the transition between regimes quite well for each of $d_o = 0.1$, 0.3 and 0.45. The lower critical flow boundary is quite robust in separating subcritical, Type I currents from Type II resonant currents. In addition, the Type II cases fall within
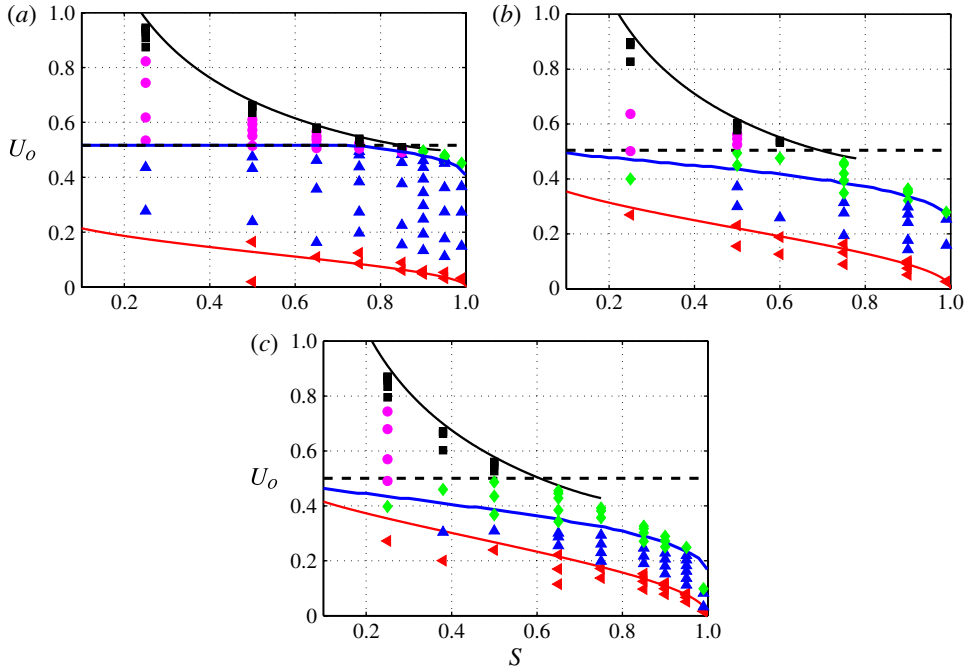
FIGURE 14. Regime diagrams plotted as U_o versus S for (*a*) $d_o = 0.1$, (*b*) $d_o = 0.3$ and (*c*) $d_o = 0.45$. Curves show the subcritical energy-conserving gravity current (red line), the maximum-amplitude gravity current/bore (blue line), the line $U_o = C_{cs}$ (black dashed line), and the conjugate state gravity current (black solid line). Symbols show numerical results by regime type, as in figure 13.

the resonant band predicted by the gravity current/bore theory. Type III rarefactions fall for the most part between the resonant band and the upper limit for critical flow ($U_o = C_{cs}$). Type IV and V gravity currents fall within the supercritical region $U_o > C_{cs}$. There is some 'fuzziness' in the bounding curves. For example, some undular bore solutions lie outside the boundary of the resonant band for $d_o = 0.1$ and some rarefactions lie within the resonant band for $d_o = 0.3$ and $d_o = 0.45$. Some of this variability is probably due to uncertainty in estimating h in the simulations. In addition, the precise transition between Type II and Type III behaviour is difficult to distinguish in the numerical results. Nonetheless, the general trends are captured for each d_o. The resonant band is largest for $d_o = 0.1$ and decreases for increasing d_o. Consequently, the region in which rarefactions are found is largest for $d_o = 0.45$ and decreases with decreasing d_o.

It is also informative to plot the regime diagrams as U_o versus S, as this removes the uncertainty in the estimates of h. These plots are shown in figure 14. Here the lower (red) and upper (black) curves are the subcritical and fastest energy-conserving gravity current solutions, respectively, first derived by Holyer & Huppert (1980) and plotted in figure 2(*b*). The upper curve corresponds to the conjugate state gravity currents found in White & Helfrich (2008) for arbitrary stratification. First notice that the subcritical energy-conserving curve is a good approximation to the transition between Type I (subcritical) and Type II (resonant) behaviour. This energy-conserving gravity current is the largest-amplitude subcritical solution. Beyond this solution, upstream bores are

found, as consistently shown in figure 14 for each d_o. The upper limit of the resonant wedge (the maximum amplitude bore solution) is shown in blue. This curve divides the Type II (undular bore) and Type III (rarefaction) simulations quite well. As shown in the (h, U_o) plots, this dividing line is not perfectly sharp, but is quite consistent across changes in d_o. For example, as predicted, the resonant band in U_o is smallest for $d_o = 0.45$ and largest for $d_o = 0.1$. It is clear that rarefactions occupy the space between the maximum bore solution and the $U_o = C_{cs} = 0.5$ horizontal line, the upper boundary for critical flow. This region is largest for $d_o = 0.45$, but for $d_o = 0.1$ it shrinks to a small range near $S = 1$. Despite being quite small for $d_o = 0.1$ (and very few rarefactions being observed in the numerical results), the theoretical curve predicts the transition from Type II to Type III quite well even for this case. Beyond $U_o = C_{cs}$, only supercritical Type IV and V solutions are found, as theory predicts.

Finally, the supercritical Type V gravity currents approach the energy-conserving conjugate state gravity current (the upper black line) in the limit of large lock height (h_d). The same result was found for gravity currents in arbitrary stratification in White & Helfrich (2008), and the two-layer cases show this as well. However, as seen in figure 14, and discussed in § 2.4, the conjugate state curve exists only for a limited range $S < S_c$. Above it, there are no energy-conserving gravity currents of finite h, only the conjugate bore, with speed C_{cs}. In addition, as the figure shows, there is a small range for which the conjugate state speed is less than C_{cs} (for example $d_o = 0.45$ between $S = 0.6$ and 0.75). In this range, since the fastest gravity current has $U_o < C_{cs}$, only rarefactions are found. However, the conjugate state solution still predicts the upper bound on U_o quite well, as was also shown in figure 12(*c,e*). For $S > S_c$, there is no theory available for the large-lock-height limit for U_o, which corresponds to a rarefaction.

7. Energetics

An important question about gravity current propagation in stratification is how much energy is transferred from the density front to the upstream internal waves/bores. This has significant implications for wave generation, energy fluxes, and mixing in ocean and atmosphere environments. It has been hypothesized (Ungarish & Huppert 2006, for constant N) that the energy transfer from a gravity current to upstream waves should be small. The hydraulic theory we have presented allows for an estimate to be made of the energy transfer between the current and the upstream two-layer system.

We take a control volume that encompasses the region behind the current front to the undisturbed upstream ambient (between sections 1 and 2 in figure 1*b*; see also figure 11) in a frame of reference moving with the front speed U_o. The total energy balance

$$\frac{\partial}{\partial t} \int_V E \, \mathrm{d}V = - \int_V \boldsymbol{\nabla} \cdot (\boldsymbol{u}E) \, \mathrm{d}V - D, \qquad (7.1)$$

where $E = (1/2)\boldsymbol{u} \cdot \boldsymbol{u} + p + bz$ is the total energy and D is the total viscous dissipation within the control volume V. Because the control volume is fixed and encompasses the full depth, (7.1) simplifies to

$$\frac{\partial}{\partial t} \int_V E \, \mathrm{d}V = \int_2 U_o E_o(z) \, \mathrm{d}z - \int_1 u_1(z) E_1(z) \, \mathrm{d}z - D, \qquad (7.2)$$

where the subscripts 1 and 2 denote that quantities are evaluated through the vertical cross-sections behind the current and through the ambient, respectively. Note that in

the moving frame of reference the ambient speed is U_o toward the current (taken here as the positive x-direction). In this frame of reference the energy in the upstream ambient is $E_o = (1/2)U_o^2 + p + bz = (1/2)U_o^2 + d_o$ for $z \leqslant d_o$ and $(1/2)U_o^2$ for $z > d_o$. The total energy flux through the cross-section is $E_{fo} = \int_2 U_o E_o \, \mathrm{d}z = (1/2)U_o^3 + U_o d_o^2$, which may be interpreted as the energy flux required to hold the gravity current fixed, or the total energy flux. The total rate of energy lost from the current, relative to the total E_{fo}, is the difference in energy flux between the ambient and the region behind the gravity current,

$$\Delta E_f = E_{fo} - \int_1 u_1(z)E_1(z) \, \mathrm{d}z = \frac{\partial}{\partial t} \int_V E \, \mathrm{d}V + D, \qquad (7.3)$$

where a positive value of ΔE_f represents a net rate of loss (and for a steady, energy-conserving gravity current $\Delta E_f = 0$). Note that even though the control volume is constant and the front is steady, the time-dependent term is appreciable due to the propagation of the upstream bore within the control volume. In the hydraulic theory, the dissipation D can be decomposed into the loss across the gravity current front D_c, from (3.8), and the dissipation across the bore D_b, from (3.2),

$$\Delta E_f = \frac{\partial}{\partial t} \int_V E \, \mathrm{d}V + D_c + D_b. \qquad (7.4)$$

This shows that the total energy transferred from the gravity current to the upstream flow is the sum of (*a*) the inviscid transfer to the propagating bore/internal waves, (*b*) the dissipation over the gravity current front and (*c*) the dissipation across the bore.

The total flux can be calculated directly by substituting $u_1(z)$ and $E_1(z) = (1/2)u_1(z)^2 + p_1(z) + bz$, evaluated through the cross-section 1, behind the gravity current front, into (7.3). To obtain the pressure at $z = 0$ below the gravity current, the Bernoulli equation is applied twice, first between sections 2 and 3 in the bore reference frame and then between sections 1 and 3 in the gravity current frame (refer to figure 1), to yield

$$p_C = p_D + \tfrac{1}{2}(U_o + C_b)^2 - \tfrac{1}{2}(U_{11} + C_b)^2 + \tfrac{1}{2}U_{11}^2. \qquad (7.5)$$

With the hydrostatic pressure, $p_1(z) = p_C - bz$, and using $p_D = d_o$, the energy flux through the current can be integrated,

$$\int_1 u_1(z)E_1(z) \, \mathrm{d}z = U_o \left[d_o + \frac{1}{2}(U_o + C_b)^2 - \frac{1}{2}(U_{11} + C_b)^2 + \frac{1}{2}U_{11}^2 \right]$$
$$- \frac{h(1-S)}{S} U_{1c} d_{1c} - \left(\frac{h}{S} + d_{1c} \right) d_{2c} U_{2c} - \frac{1}{2}U_{1c}^3 d_{1c} - \frac{1}{2}U_{2c}^3 d_{2c}, \quad (7.6)$$

to yield the total rate of energy loss, $\Delta E_f = E_{fo} - \int_1 u_1(z)E_1(z) \, \mathrm{d}z$. As a result, each of the three terms in (7.4) can be evaluated.

We calculate ΔE_f from the numerical simulations by integrating the energy flux through the cross-sections 1 and 2 (as shown in figure 11). The integral through section 1 is an average in x over the region in which $\overline{h}$ is calculated (bounded by, say, x_1 and x_2) and in time (from $t_1 = 30$ to $t_2 = 60$), so that the total energy loss in the simulations is

$$\Delta E_f = E_{fo} - \frac{1}{(t_2 - t_1)} \frac{1}{(x_2 - x_1)} \int_{t_1}^{t_2} \int_{x_1}^{x_2} \int_0^1 u(x, z, t)E(x, z, t) \, \mathrm{d}z \, \mathrm{d}x \, \mathrm{d}t, \qquad (7.7)$$
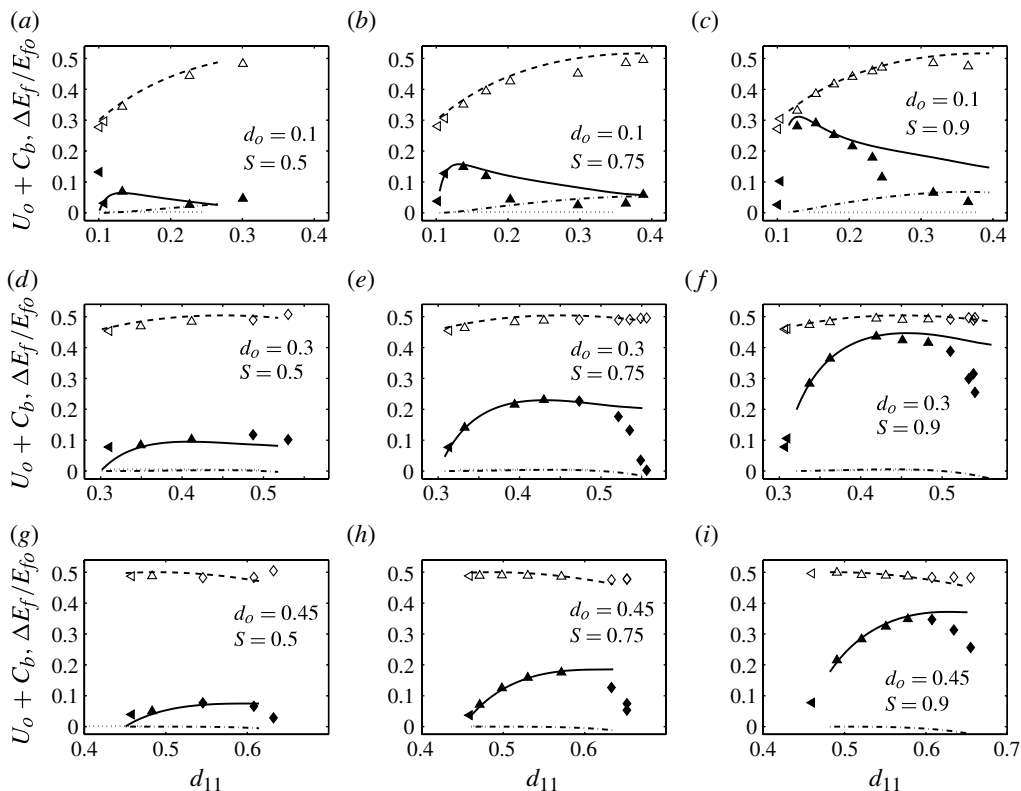
FIGURE 15. Energy transfer from the gravity current ΔE_f, normalized by its total energy flux E_{fo}, versus bore amplitude d_{11}. (*a–c*) $d_o = 0.1$, (*d–f*) $d_o = 0.3$, (*g–i*) $d_o = 0.45$; (*a,d,g*) $S = 0.5$, (*b,e,h*) $S = 0.75$, (*c,f,i*) $S = 0.9$. Hydraulic theory (solid black line) and numerical results (solid symbols, where shape corresponds to regime type as in figure 13). Also shown are the hydraulic theory for D_c (dotted line) and D_b (dot-dashed line). Bore speed, $U_o + C_b$, in the laboratory frame versus d_{11} is also shown (dashed line, Klemp *et al.* (1997) closure; open symbols, numerical results).

where $u(x, z, t)$ and $E(x, z, t)$ are both calculated in the frame of reference moving with gravity current speed U_o. This expression can be directly compared with the hydraulic theory. However, it is difficult to decompose the numerical results into the three components of (7.4), so we calculate only the total energy transfer, ΔE_f.

The results for the total rate of energy transfer from the gravity current to the upstream flow is shown in figure 15, where the numerical results for ΔE_f are shown as a function of bore amplitude d_{11}, for a range of d_o and S. For comparison the predictions from hydraulic theory are shown for ΔE_f, D_b, and D_c. For ΔE_f and D_b the curves corresponding to the energy-conserving gravity current front, $D_c = 0$, are shown, whereas to give an upper bound for the gravity current dissipation, the D_c curve that maximizes the function $D_c(d_{11})$ is shown (cf. figure 3*a,b*). The energy transfer is normalized by E_{fo} in order to show the fraction of total energy lost from the gravity current. Also shown is the bore speed in the laboratory frame, $U_o + C_b$, versus d_{11} with the Klemp *et al.* closure (3.1) for comparison.

The comparison between the theory and simulations is quite favourable across the (d_o, S) parameter space. The results show that the energy loss increases with bore amplitude before reaching a maximum and subsequently decreasing. The maximum value of $\Delta E_f / E_{fo}$ is well predicted by the theory for each case. The maximum fraction of the gravity current energy lost ranges from less than 10 % for $d_o = 0.1$, $S = 0.5$, to over 40 % for $d_o = 0.3$, $S = 0.9$. In general the energy transfer increases as $S \to 1$ but is maximized at an intermediate value of d_o. This maximum in the $\Delta E / E_{fo}$ curve occurs because the energy transfer depends not just on the bore amplitude but also on C_b (the difference in the resting frame between the gravity current front speed and the bore speed). A large disturbance moving much faster than the gravity current will maximize ΔE_f, but ΔE_f decreases for large d_{11} as U_o approaches the bore speed $U_o + C_b$.

It is perhaps surprising how well the simulations match the hydraulic theory, given the assumptions of uniform layer thickness and neglect of non-hydrostatic effects associated with the undular bore. The success is likely due in part to the fact that the Klemp *et al.* (1997) closure successfully captures the properties of the numerical bores, as seen in the comparison of $U_o + C_b$ versus d_{11} between the theory and numerics in figure 15. The closure matches the simulated bore speeds across all cases where upstream undular bores are observed (and even some rarefaction and subcritical cases, which are also shown for comparison). As discussed previously, the large-amplitude limit of the gravity current/bore solutions can exceed the conjugate bore, $d_{11} = 0.5$, $C_{cs} = 0.5$. The jump condition continues for $d_{11} > 0.5$, and this region continues to show good agreement with the numerical results, in particular for larger d_o. For $d_o = 0.45$ the majority of the bore solutions have $d_{11} > 0.5$. Even though for $d_{11} > 0.5$, $D_b < 0$ (implying energy is required rather than dissipated), the gravity current provides the required energy transfer, as shown by the fact that $\Delta E_f > 0$ for these cases. These results support the use of the energy-conserving closure. This is perhaps not surprising in the present problem, where the upstream disturbance consists of waves.

The success of the hydraulic theory suggests that energy transfer is largely inviscid. This is verified by comparing D_b and D_c with the total energy loss. In all cases, the gravity current dissipation, D_c, is insignificant, at least two orders of magnitude smaller than ΔE_f. This explains why the $\Delta = 0$ assumption matches the upstream bore results so well (as in figure 12). It appears that dissipation over the front is a negligible component of the energy transfer. The bore dissipation, D_b, is significant for $d_o = 0.1$, but not for $d_o = 0.3$ or 0.45. This suggests that the dominant component of the energy transfer is the term $\partial/\partial t \int_V E \, dV$, which is largely inviscid and represents the energy required to change the upstream state ahead of the gravity current and drive the undular bore. The theory and numerical results verify that this energy transfer is significant, requiring as much as 40 % of the total energy of the gravity current to sustain the bore. Capturing this transfer is necessary to the prediction of the gravity current front speed relationship, U_o versus h, in the resonant regime, and it has been demonstrated that the hydraulic theory accomplishes both tasks quite well. The significant energy transfer to waves in the two-layer case is in contrast to the results of Ungarish & Huppert (2006), who found negligible transfer in uniform stratification. A possible explanation for this distinction is that a Boussinesq fluid with uniform stratification does not support internal solitary waves of the classic KdV type; however, nonlinear internal waves governed by a related equation are possible (Grimshaw & Yi 1991). This seems consistent with Munroe *et al.* (2009), who found significant energy transfers (up to 22 %) to upstream disturbances in a linearly stratified system.

8. Discussion and summary

The hydraulic theory and simulations described here illustrate the complexity of frontal dynamics for a gravity current propagating into a two-layer stratified ambient. The regimes, organized by their Froude number $Fr = U_o/c_o$ and thickness, are shown to be analogous to critical flow over solid topography, but are more complex because the front is a free boundary. As a result, the gravity current is subject to an additional momentum constraint. By imposing this constraint as well as closures on energy dissipation over the gravity current front and modelling the connection to an upstream undular bore, we have found that the theory is robust in predicting the occurrence of the various frontal regimes observed in numerical simulations as a function of Fr and h.

A second result of the theory is the prediction of a relationship between the front speed U_o and thickness h across the full range of regime types. The theory builds, in particular, on that of Holyer & Huppert (1980), Rottman & Simpson (1989) and White & Helfrich (2008) to yield predictions for gravity current front speed in subcritical and supercritical regimes, as well as the resonant regime in which an upstream bore is generated by the current. The energy and internal bore closures give the correct behaviour in the large-amplitude bore limit. Moreover, the results show that the upper limit separating resonant generation from supercritical flow is the conjugate bore, $C_{cs} = 0.5$, $d_{11} = 0.5$, as demonstrated by Stastna & Peltier (2005) for solid topography.

An analysis of the energy budget for the hydraulic theory and numerical results shows that for a two-layer ambient, a substantial fraction of the energy flux of the gravity current can be transferred to the upstream bore. This has significant implications for the generation of nonlinear internal waves in the atmosphere and coastal river plumes. Questions remain about dissipation due to turbulent mixing, for which very high rates have been observed in the ocean near river plume fronts. Neither the hydraulic theory nor the numerical simulations capture this process, which requires some combination of careful laboratory experiments and three-dimensional direct numerical simulation to understand.

The results confirm that the generation of nonlinear internal waves at the gravity current front is due to transcritical resonance, which is well predicted by the hydraulic theory. The implications are that there is a distinct band of Fr for a given h, S, d_o for which upstream internal waves are generated. This is in contrast to the hypothesis that waves are generated when $Fr < 1$ and the front is supercritical for $Fr > 1$. As we have seen, the fairly simple criterion $U_o/C_{cs} > 1$ controls the transition to supercritical flow, but the finite resonant band in U_o requires linking the gravity current to the upstream bore.

While the present theory is limited to two-layer stratification, we remark that recent results (Camassa & Tiron 2011) have shown that some properties of internal wave propagation in continuous stratification can be well approximated by an equivalent two-layer system optimally matched in terms of long-wave charactertics such as the phase speed. This opens the possibility of applying the present theory as a more general framework in continuously stratified fluids, particularly in the coastal ocean, where a very thin surface layer typically exists. However, the existence of breaking and trapped core formation where there is appreciable near-surface stratification, in addition to higher vertical wave modes, may in some cases substantially alter the behaviour.

As an example, the observations by Nash & Moum (2005) of nonlinear internal waves at the Columbia front were made in approximately 40 m of water where the plume thickness was of the order 5 m, roughly corresponding to $h \approx 0.1$ in

non-dimensional units. Based on their figure 3(*a*), near the front the ambient density difference from top to bottom was approximately 5 psu. They calculated a wave speed of approximately $c_o \approx 0.4$ m s^{-1}, which corresponds to $c_o/\sqrt{g'H} \approx 0.3$, or an equivalent two-layer system with $d_o \approx 0.1$. The density difference between the plume and the bottom was about 13 psu, yielding a value of $S \approx 0.4$. They observed the onset of wave generation when U_o was less than ≈ 0.5 m s^{-1}, or ≈ 0.35 in non-dimensional units. This is certainly within the resonant band shown in figure 14. It may be possible to improve the prediction for the precise onset of wave generation by more precise matching of the ambient density profile to its optimal two-layer counterpart. We also remark that the possibility remains to extend the full two-layer theory with an upstream bore to continuous profiles as well to incorporate ambient velocity shear.

Acknowledgements

REFERENCES

BAINES, P. G. 1984 A unified description of two-layer flow over topography. *J. Fluid Mech.* **146**, 127–167.

BAINES, P. G. 1995 *Topographic Effects in Stratified Flows*. Cambridge University Press.

BELL, J. B. & MARCUS, D. L. 1992 A second-order projection method for variable-density flows. *J. Comput. Phys.* **101**, 334–348.

BENJAMIN, T. 1968 Gravity currents and related phenomena. *J. Fluid Mech.* **31**, 209–248.

BROWN, D. J. & CHRISTIE, D. R. 1998 Fully nonlinear solitary waves in continuously stratified incompressible Boussinesq fluids. *Phys. Fluids* **10**, 2569–2586.

CAMASSA, R. & TIRON, R. 2011 Optimal two-layer approximation for continuous density stratification. *J. Fluid Mech.* **669**, 32–54.

CHEONG, H.-B., KUENEN, J. J. P. & LINDEN, P. 2006 The front speed of intrusive gravity currents. *J. Fluid Mech.* **552**, 1–11.

CHU, V. H. & BADDOUR, R. E. 1977 Surges, waves and mixing in two-layer density stratified flow. In *17th Congress of the International Association on Hydraulic Research, Baden-Baden, Germany*, pp. 303–310. IAHR.

CROOK, N. 1983 The formation of the Morning Glory. In *Mesoscale Meteorology: Theories, Observations, and Models* (ed. D. Lilly & T. Gal-Chen). D. Reidel.

DERZHO, O. G. & GRIMSHAW, R. 1997 Solitary waves with a vortex core in a shallow layer of stratified fluid. *Phys. Fluids* **9**, 3378–3385.

ESLER, J. G. & PEARCE, J. D. 2011 Dispersive dam-break and lock-exchange flows in a two-layer fluid. *J. Fluid Mech.* **667**, 555–585.

FARMER, D. & ARMI, L. 1999 The generation and trapping of solitary waves over topography. *Science* **283**, 188–190.

FLYNN, M. R., UNGARISH, M. & TAN, A. W. 2012 Gravity currents in a two-layer stratified ambient: the theory for the steady state (front condition) and lock-released flows, and experimental confirmations. *Phys. Fluids* **24**, 026601.

GRIMSHAW, R., CHAN, K. & CHOW, K. 2002 Transcritical flow of a stratified fluid: the forced extended Korteweg–de Vries model. *Phys. Fluids* **14**, 755–774.

GRIMSHAW, R. & SMYTH, N. 1986 Resonant flow of a stratified fluid over topography. *J. Fluid Mech.* **169**, 429–464.

GRIMSHAW, R. & YI, Z. 1991 Resonant generation of finite-amplitude waves by the flow of a uniformly stratified fluid over topography. *J. Fluid Mech.* **229**, 603–628.

HELFRICH, K. & WHITE, B. 2010 A model for large-amplitude internal solitary waves with trapped cores. *Nonlinear Process. Geophys.* **17**, 303–318.

HOLYER, J. Y. & HUPPERT, H. E. 1980 Gravity currents entering a two-layer fluid. *J. Fluid Mech.* **100** (4), 739–767.

KILCHER, L. F. & NASH, J. D. 2010 Structure and dynamics of the Columbia river tidal plume front. *J. Geophys. Res.-Oceans* **115**, C00B12.

KING, S. E., CARR, M. & DRITSCHEL, D. G. 2010 The steady-state form of large-amplitude internal solitary waves. *J. Fluid Mech.* **666**, 477–505.

KLEMP, J., ROTUNNO, R. & SKAMAROCK, W. 1997 On the propagation of internal bores. *J. Fluid Mech.* **331**, 81–106.

LAMB, K. G. 1994 Numerical experiments on internal wave generation by strong tidal flow across a finite amplitude bank edge. *J. Geophys. Res.* **99**, 843–864.

LAMB, K. G. 2000 Conjugate flows for a three-layer fluid. *Physics of Fluids* **12**, 2169.

LAMB, K. G. 2002 A numerical investigation of solitary internal waves with trapped cores formed via shoaling. *J. Fluid Mech.* **451**, 109–144.

LAMB, K. G. & WILKIE, K. P. 2004 Conjugate flows for waves with trapped cores. *Phys. Fluids* **16**, 4685–4695.

LAWRENCE, G. 1993 The hydraulics of steady two-layer flow over a fixed obstacle. *J. Fluid Mech.* **254**, 605–633.

LONG, R. 1954 Some aspects of the flow of stratified fluids. Part 2. Experiments with a two-fluid system. *Tellus* **6**, 97–115.

MARINO, B., THOMAS, L. & LINDEN, P. 2005 The front condition for gravity currents. *J. Fluid Mech.* **536**, 49–78.

MAXWORTHY, T., LEILICH, J., SIMPSON, J. E. & MEIBURG, E. H. 2002 The propagation of a gravity current into a linearly stratified fluid. *J. Fluid Mech.* **453**, 371–394.

MELVILLE, W. K. & HELFRICH, K. R. 1987 Transcritical two-layer flow over topography. *J. Fluid Mech.* **178**, 31–52.

MOUM, J., NASH, J. & KLYMAK, J. 2008 Small-scale processes in the coastal ocean. *Oceanography* **21** (4), 22–33.

MUNROE, J. R., VOEGELI, C., SUTHERLAND, B., BIRMAN, V. & MEIBURG, E. 2009 Intrusive gravity currents from finite-length locks in a uniformly stratified fluid. *J. Fluid Mech.* **635**, 245–273.

NASH, J. D., KILCHER, L. F. & MOUM, J. N. 2009 Structure and composition of a strongly stratified, tidally pulsed river plume. *J. Geophys. Res.-Oceans* **114**, C00B12.

NASH, J. D. & MOUM, J. N. 2005 River plumes as a source of large-amplitude internal waves in the coastal ocean. *Nature* **437**, 400–403.

PAN, J. & JAY, D. A. 2009 Dynamic characteristics and horizontal transports of internal solitons generated at the Columbia river plume front. *Cont. Shelf Res.* **29** (1), 252–262.

ROTTMAN, J. & SIMPSON, J. 1989 The formation of internal bores in the atmosphere: a laboratory model. *Q. J. R. Meteorol. Soc.* **115**, 941–963.

SIMPSON, J. E. 1997 *Gravity Currents: In the Environment and the Laboratory*, second edition. Cambridge University Press.

STASHCHUK, N. & VLASENKO, V. 2009 Generation of internal waves by a supercritical stratified plume. *J. Geophys. Res.* **114** (C1), 1–17.

STASTNA, M. & LAMB, K. 2002 Large fully nonlinear internal solitary waves: the effect of background current. *Phys. Fluids* **14**, 2987–2999.

STASTNA, M. & PELTIER, W. R. 2005 On the resonant generation of large-amplitude internal solitary and solitary-like waves. *J. Fluid Mech.* **543**, 267–292.

TAN, A. W., NOBES, D. S., FLECK, B. A. & FLYNN, M. R. 2011 Gravity currents in two-layer stratified media. *Environ. Fluid Mech.* **11**, 203–223.

UNGARISH, M. 2006 On gravity currents in a linearly stratified ambient: a generalization of Benjamin's steady-state propagation results. *J. Fluid Mech.* **548**, 49–68.

UNGARISH, M. & HUPPERT, H. 2006 Energy balances for propagating gravity currents: homogeneous and stratified ambients. *J. Fluid Mech.* **565**, 363–380.

WHITE, B. L. & HELFRICH, K. R. 2008 Gravity currents and internal waves in a stratified fluid. *J. Fluid Mech.* **616**, 327–356.

WHITHAM, G. B. 1974 *Linear and Nonlinear Waves*. Wiley.

WOOD, I. & SIMPSON, J. 1984 Jumps in layered miscible fluids. *J. Fluid Mech.* **140**, 215–231.

YIH, C. S. & GUHA, C. R. 1955 Hydraulic jumps in a fluid system of two layers. *Tellus* **7**, 358–366.